Dear Anonymous Referee #1,

Thank you very much for your comments that certainly will improve the paper. In the following I will answer your questions and indicate which information is added to the original paper.

Overall

RC:*The paper presents CFD(URANS) simulations of the NREL 5MW wind turbine. The aim is to examine transient gusts and the associated load implications. The underlying research question is interesting with some interesting conclusions, e.g. that the presence of the tower suppress separation. However, the article appears incomplete and somewhat unfocused, hence confusing at times. The written language is mediocre and could be improved for readability. Therefore, the recommendation is to reject the paper in the current state, but encourage to resubmit at a later stage. The author addresses a number of issues in the conclusion and these should be answered for resubmission. Hence, a more clear focus should be applied, e.g. how related is the tip vortex transportation actually to the transient loading during a gust?*

AC: To improve the language, I shortened the sentences and reordered them to strictly match the subject-verb-object order. Moreover, I changed some wordings to improve the readability of the paper. This hopefully will clarify the focus on the validation of the method, which is the main purpose of the paper.
I also fixed the main issue in my conclusion, namely the validation of the resolved-gust approach. The CFD(U-RANS)-computation is now compared to FAST and shows very good agreement in flow regions with attached flow. I added the according figure to my response. Besides, everything else would mean to try to run before I can walk.

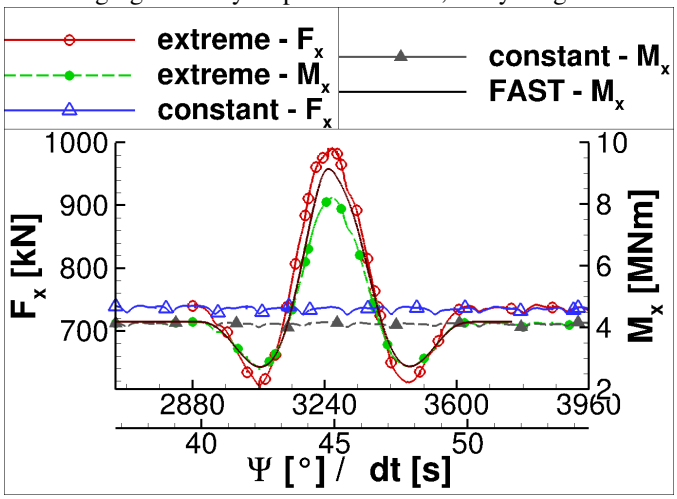

The tip vortex transport is an indication whether the method works correctly. It has little effect on the rotor loading. This information is added to section 5.3.

General Comments

1. RC: *Why are the gusts propagated with the speed of sound? This appears an odd choice as a real gust would propagate by its own velocity.*
   RC: Yes you are right. It is the weak point of the chosen modelling approach. In combination with an incompressible solver it becomes severe as the speed of sound is infinite. This point has already mentioned in section 1, page 2, line 27. The use of the field approach by Parameswaran et al. or the velocity disturbance approach would overcome this issue but introduce other problematic questions. I will expand the explanation in section 1.

2. RC:*Why is the floor modelled, but no ABL? If a no-slip condition is applied, why not have a shear? The dependence on height appears to disappear without explanation in the equations. Otherwise, investigate a uniform inflow with the turbine "suspended" in space, which would give symmetry.*
AC: To be able to introduce the ABL in future computations and to perform a comparison of both computations on the same grid, the grid has already been prepared accordingly. I added this information to section 3.2. Nevertheless, the first step in introducing a new method is to validate the simulation method as isolated as possible. Thus, the height dependency of the velocity is neglected to be able to evaluate the gust impact on the rotor aerodynamics. I added the information more clearly in the paper in section 3.1 4.1, 4.3.

3. RC: *The turbine is stiff in the computations. Is this choice appropriate when examining extreme loads, particular for large wind turbines as the 5MW? This also affects the observed symmetry in Table 1 and whether this is to be expected.*
AC: The first step in introducing a new method with interdisciplinary character is to validate each part of the method on its own. The combination with structure dynamics and/or speed controllers can only follow after the issues in remark [1] and [13] are clarified. The motivation is clarified in section 1, page 2. Moreover, a remark about the plausibility of symmetric results is added in section 5.2, 5.3.

4. RC:*Improved description of flow solver. What does dual cells, projection methods, prism layers, and C functions imply?*
AC: Dual cells imply a cell-centred scheme of the solver. With the projection method the momentum equations are first solved with an approximated pressure field and do not fulfil continuity. The pressure field is then corrected by solving a Poisson equation to fulfil the continuity conditions. The c-functions enable a high flexibility on the definition of inflow conditions on the boundaries of the flow domain. The description of THETA in section 2 is extended to answer your questions. Prism layers are part of the meshing topology.

5. RC: *Why are there meshing issues involved for the nacelle, but not the hub nor tower?*
AC: Due to the narrow gap between rotor and nacelle a valid chimera overlap-region could not be achieved. Thus the nacelle of the NREL 5MW turbine is neglected while the tower is respected. This sentence is added to section 3.2

6. RC:*How many cells in first grid?*
AC: 11.6 Mio in the chimera child grid and 13.3 Mio points in the parent grid. The information has been already on page 4, lines 20 and 26 in the first version.

7. RC:*The boundary condition definition is unclear, e.g. "the remaining farfield surface"?*
AC: It is the surfaces on top, left and right of the flow domain. I clarified this in the paper, section 3.2.

8. RC: *How is such a small gust interesting? The cos gust basically results in a TI of* 1.5% *(=(sqrt(2)/2*0.25m/s)/11.4m/s, hardly a defining design case.*
AC: It represents the turbulence level of the atmospheric flow around wind turbines as measured by Schaffarczyk et al. (2017). A remark is added at the end of section 4.2.

9. RC: *How are the characteristic times chosen? And why would they be sinusoidal?*
AC: The characteristic time for the 1-cos gust was chosen to generate an un-compressed cosinus larger than one rotor revolution and smaller than a 10s interval. The characteristic time for the EOG is taken from the IEC standard. A comment is added in the sections 4.2 and 4.3.

9. RC: *And why would they be sinusoidal? It might follow the standards, but does this correspond to measured gusts or gusts from LES?*
AC: Well, this opens up a wide research field and several attempts are made to find profound answers to this question. One example is Bierbooms et al. (1999) who investigated the gust shape from wind measurements and simulation. By the use of statistical methods they found that a sinus fairly represents gust. Alternatively, Zbrozek (1953) gives an overview on different possible gust shapes. Concerning the agreement of the standards and results from LES or field measurements, Mücke et al. (2010), for example, showed that in field measurements velocity-changes with high frequency occur. These are not represented in the IEC standard. Apart from that, the question to be answered by my

paper neither is whether or not the implemented gust corresponds to any field measurement or LES computation with the specific related uncertainties. Nor it is the purpose to answer the question how the IEC standard may be improved. The aim of the paper is to validate the resolved gust approach, which requires

- low uncertainties in the inflow conditions which is achieved by perfect control of the inflow conditions
- low uncertainties in the inflow conditions by applying a gust that is independent of the horizontal and vertical position
- comparability to results of other methods such as FAST by using well-defined inflow conditions

All of the above requirements are best matched by the IEC standard gust. The introduction of realistic fluctuations which result from LES or measurement can be applied as soon as the validation of the aerodynamics is finished, aero-elasticity has been included and a speed controller is available.

10. RC: *Explain spikes in e.g. Figure 3 around t = 3230 sec.*
AC: The high-frequency oscillations occur in a time step wherein the elliptic pressure equation has not reached the required residual of 10^{-5} in the maximum allowed number of iterations. The number of iterations were chosen to guarantee an efficient computation of the test case. The information about the criteria is added to section 2. Moreover, a remark on the high-frequency oscillations is added to section 5.1.

11. RC: *Is the use of average loads correct? Most people use equivalent loads.*
AC: To be able to compute and discuss equivalent loads assumptions on the wind field, wind velocity bins and statistics have to be included to the discussion in the paper. This would create new questions and unnecessary uncertainties to the results. Therefore I included a more profound comparison of averaged and peak loads to section 5.2 that clarifies the introduction of the averaged gust loads.

12. RC: *Details are difficult to see in Figures 7-12.*
AC: I modified the figures to better illustrate the content. Moreover, I enlarged the figures.

13. RC: *In terms of experiments, why not validate the setup against the MEXICO experiments or Krogstad as there is nothing "special" about the NREL 5MW.*
AC: The validation of the setup against any experiment is not a matter of question because a validation against the NREL 5MW is performed in section 5.1 and a successful validation of THETA against the NREL phase VI UAE has been presented by Länger-Möller in 2017. It is the gust simulation that needs validation. Meanwhile I found a possibility to validate the gust simulation against FAST results. I included the results to figure 5 and according comments to section 5.3. The Conclusion in section 6 has been changed accordingly.

14. I added a short description of FAST and the modelling approaches in section 2. That includes a modification of the section title to "Numerical methods" and a shift of the former section 2 to 2.1

Technical corrections:

1. RC: *Why are all references written twice? Please correct.*
AC: References are now written once.

2. RC: *Wording is often rather strange, e.g. use of "regarding", "promising"(page 3, line 27), "respecting",*
AC: I changed the wording you indicated.

3. RC: *Sentences are back-to-front, e.g. page 2, line 9-10. Please correct*
AC: I changed the wording in sentences on page 2, line 9-10 and some other back-to-front sentences.

4. RC: . *Consistency. On page 2, there are mentioned "CFD" several times, while aero-elastic tools are denominated. Please also specify which CFD tools were used as there are large differences between "CFD" tools.*
   AC: I specified the used CFD tools more clearly. This implies the title. Moreover I added a short description of the most popular aero-elastic wind turbine tools.

5. RC: *Periodic and initial is not the same(page 7, line 15).*
   AC: Of course, periodic and initial is not the same. But the periodic state of the flow field is mandatory as starting (initial) conditions to start a gust-computation. I clarified this in the mentioned paragraph.

Moreover, I performed the following changes:

- I changed the word "hexahedra" to "hexagon"
- I adapted wind velocity to wind speed
- I adapted gust speed to gust velocity

throughout the entire paper.

Dear Dear Anonymous Referee #2,

thank you very much for your hints to improve the analysis of my results. I especially appreciated the recommendation of references. Furthermore I will answer your questions.
As I introduced a validation of the computation as response to Referee #1, section 2 now contains two subsections. The first one for THETA, the second to describe the simulation setup in FAST.

Overall

- RC: *The article describes a CFD approach to gust modelling for wind turbines, presenting some interesting results. As the CFD model is incompressible, any change in velocity in the domain is instantaneously influencing the full domain. As a consequence, the gust is not travelling through the domain, but the velocity is basically increasing everywhere in the domain instantaneously. The consequence of this with respect to the wake development should be discussed.*
  AC: Yes. Indeed, the entire vortex-transport discussion is turning around this point. To clarify this I added the paragraph "In consequence to the infinite speed of sound in the entire flow domain, the velocity in the field changes gradually. Thus, the vortices that are shed from the blade at a given wind speed are not transported with their specific transport velocity. Contrariwise, all existing vortices experience identical changes in the transport velocity. In consequence, the geometrical distance between existing vortices remains constant." to section 5.3.

- RC: *Additionally, the assumption of infinite mass and inertia along with a non-elastic model might also have quite large effects, and should be discussed.*
  AC: Yes you are right. A finite mass and inertia would reduce the rotor loading during the gust. Moreover, elastic deformation during the gust becomes important in the given test case and would destroy the symmetry in the rotor loading. These trends can be seen by switching on the according models in FAST. Nevertheless, the motivation of the paper has been to validate the resolved gust approach in THETA. In this context it is best to diminish the uncertainties by reducing the model complexity. This is done by isolating the aerodynamic effects. The discussion of results is enhanced by the information to trends for finite mass and inertia (section 5.2, 5.3). Section 1 now contains a more precise definition of the scope of the paper.

- RC: *Finally, the ABL is neglected along with any turbulence, which is also indicated by other reviewers could be much larger than the cosines gust.*
  AC: The cosines-gust represents the turbulence level of the atmospheric flow around wind turbines as measured by Schaffarczyk et al. (2017). A remark is added at the end of section 4.2. The ABL inflow profile can be added after the resolved-gust approach has been validated successfully. This point is clarified in the paper in section 3.1, 4.1, 4.3.

Figures

- RC: *Generally the figures are very small, and Figure 1 about the grid set-up is basically of no use and should be replaced.*
  AC: I enlarged the figure. Moreover I changed the content to represent the chord-wise distribution, span-wise distribution

in the blade tip region and the meshing topology in the farfield. I attached the figure to my response.

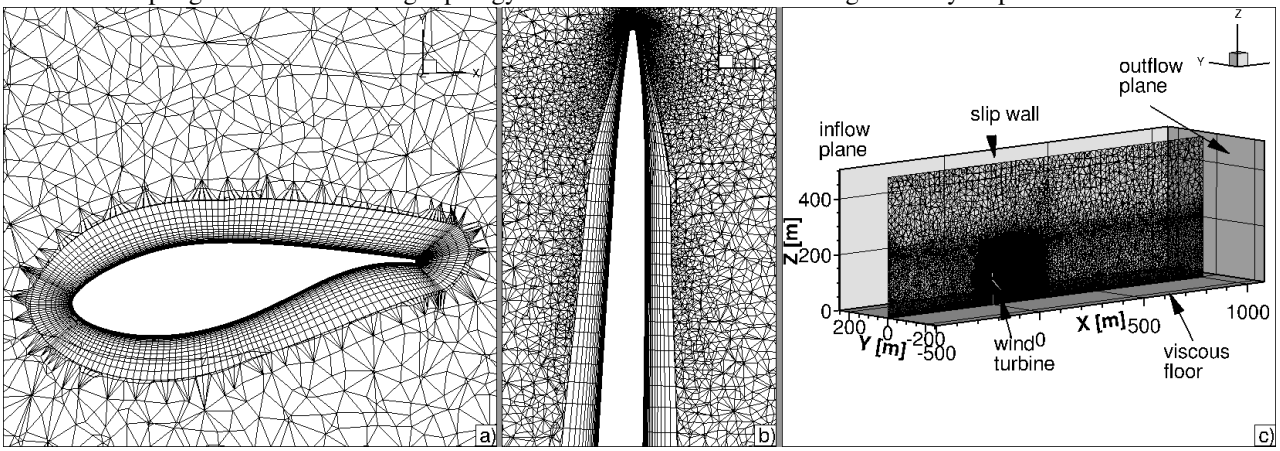

– RC: *The Cp and Cf plots, Fig. 7,8,9,10, 11 and 12 are very small and not providing that much information.*
AC: I enlarged figure 7 to 12 and summarized them into 3 figures to enable a better comparison between no tower/tower blockage. I added one exemplary figure to my response. The descriptive text in the paper changed accordingly.

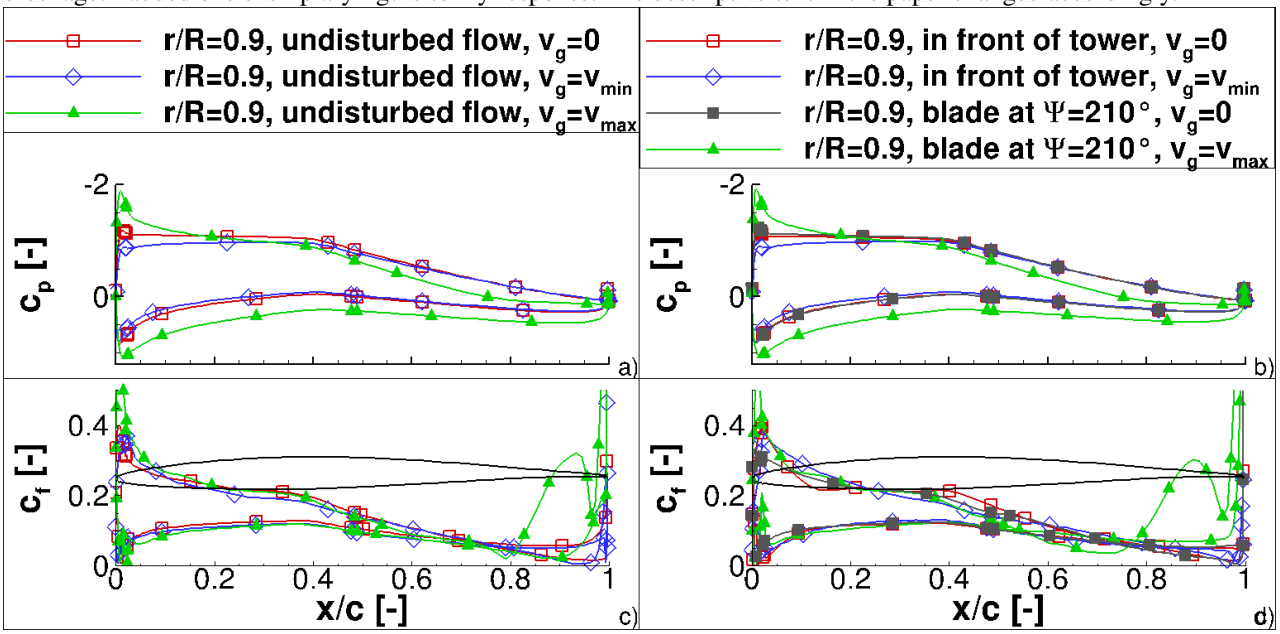

– RC: *They could be exchanged with plots of radial force distributions at [0,90,180,270] degrees azimuth. Eventually, a blow-up of the Cf distribution could be included to assist the discussion about separation versus no separation.*
AC: I added a plot of the radial distribution of rotor thrust and torque to the paper. Please refer to section Results, bullet-point 1 for further information.

– RC: *In Figure 13, the choice of blue and black color is not optimal, red would be easier to distinguish from the black.*
AC: I changed the colouring from blue to red.

Flow solver

- RC: *The description of the flow solver setup is very sparse and should be extended. What time integration is used for the present work, and what size of time step is used.*
  AC: Eulerian Implicit time stepping scheme, global time stepping. The information is added. A time step of $0.006887052s$ is used which is equivalent to a rotor advance of $\delta\Psi = 0.5°$. The information has partly been at the end of section 2 but is expanded.

- RC: *It is stated that a second order central scheme is used, but it seems highly unrealistic that this can be done without generating wiggles for this high a Reynolds number without some artificial damping. Please explain.*
  AC: Please refer to page 3, line 13: "Pressure stabilization is used to avoid spurious oscillations caused by the collocated variable arrangement." This pressure stabilization prevents the central scheme from oscillating. No further comment is made in the paper.

- RC: *The present reviewer is well aware of the no-slip wall conditions used, but I do not understand how it differs from the viscous wall condition prescribed at the earth surface. Should it be an inviscid wall or slip conditions at the earth surface?*
  AC: It has been a typing error in page 4, line 22. The floor is a viscous wall but the top, left, and right surface of the flow domain are slip walls. I changed the word no-slip to slip in the given line.

Grid characteristics

- RC: *The description is not accurate and do not even include any description of the gridding of the tower component.*
  AC: The tower surface grid is meshed structured in a height below $5\,\mathrm{m}$ with 54 point in height and 180 points in radial direction. Above this grid, a triangulated unstructured grid is generated. The maximum edge length is $0.55\,\mathrm{m}$. As the tower surface is modelled as slip-wall, tetrahedrons are built directly on the tower surface. This information is added to section 3.2.

- RC: *Additionally, some more details about the issues related to including the nacelle in the grid should be given.*
  AC: Due to the narrow gap between rotor and nacelle a valid chimera overlap-region could not be achieved. Thus the nacelle of the NREL 5MW turbine is neglected while the tower is respected. This sentence is added to section 3.2

- RC: *The chord-wise resolution is on the coarse side; normally more than 250 cells are needed for an accurate resolution of the flow development. Are the results at all close to grid independent?*
  AC: In Länger-Möller (2017) it has been shown that with even coarser distribution in chord-wise direction, the results of THETA matched the NREL UAE phase VI perfectly. Based on this findings the mesh of the NREL 5MW turbine was generated. Moreover, the very good agreement to the NREL 5MW documentation of Jonkman et al. (2009) (section 5.1) indicate that the grid is fine enough.

- RC: *More illustrative figures showing the chord-wise and span-wise resolution should be included, along with a cut through the full grid topology.*
  AC: See section Figures, first bullet point.

Results

- RC: *Generally, the pressure distributions add very little information to the discussion, and should be replaced by span-wise force distributions.*
  AC: Thank you for the suggestion. I prepared figures of the span-wise force distribution and added them to the paper. It

is also attached to my reply. In the paper, a new paragraph is added to section 5.3.

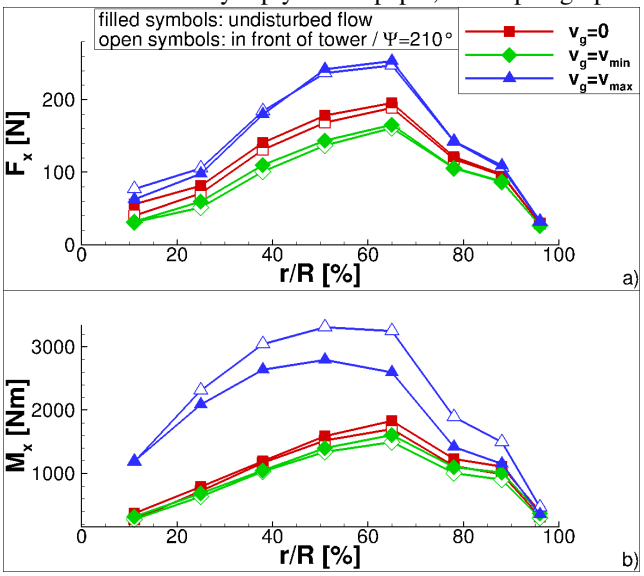

– RC: *Figure 13 on the tip vortex movement is very hard to interpret, as we do not know if the rotor is at identical azimuth positions for the different snap-shots.*
AC: Yes, the instances were taken at identical azimuth positions. This information is added to section 5.3.

– RC: *It would maybe be more interesting to show the axial and radial location of the tip-vortex as function of vortex age at the three instances in time.*
AC: I changed figure 14 accordingly to your suggestions and added a plot of the axial and radial location of the tip vortex as function of vortex age. Conversely, I only changed the colouring of figure 13 from blue to red. I attached the figures to give you an impression. The description of the figures changed accordingly in section 5.3.

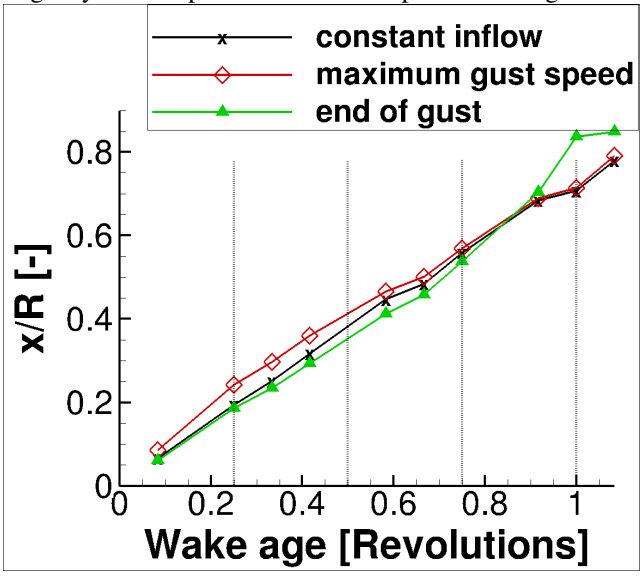

References

- RC: *The major references to CFD for wind turbines are very recent; CFD for wind turbines track back to the late nineties which I believe should be reflected.*
  AC: I summarized the milestones in CFD for wind turbines in some additional sentences right at the beginning of section 1. I namely refer to Soerensen and Hansen (1998), Soerensen et al. (2002), Johansen et al. (2002), Bazilevs et al. (2011), Hsu et al. (2012), and Chow and van Dam (2012).

- RC: *Additionally, the author chose to refer to secondary references eg. Kessler and Löwe 2012, where the reference to Zhang et al from my point of view should be preferred. P3, L15 moving grid blocks (Zhang et al. 2007) as implemented by (Kessler and Löwe 2012).*
  AC: I followed your suggestion and additionally added a reference to Pan et al. (2002). The information is added to section 2.1.

- RC: *Another example is the reference for the usage of k-omega model for wind turbines which has been pioneered by others in the late nineties, e.g. Rotor performance prediction using a Navier-Stokes Method, Sørensen and Hansen, AIAA-98-0025.*
  AC: I never intended to state that Länger-Möller pioneered the Menter SST model for wind turbine applications. Anyway, I clarified that during the validation of THETA by Länger-Möller et al. (2017) the Menter-SST model has been the most accurate turbulence model. Thus it is used in the present study. The information will be given in section 2.1.

List of changes to the original paper

To improve the original paper, the following changes have been made:

Modification of Text

- I corrected the language wherever it was necessary (recommendation by Anonymous Reviewer #1)
- I changed the word "hexahedra" to "hexagon"
- I adapted wind velocity to wind speed
- I adapted gust speed to gust velocity
- I corrected the display of citations (requested by Anonymous Reviewer #1)
- I added a description of older CFD literature in the preamble (suggestion by Anonymous Reviewer #2)
- I added a description of the aero-elastic tools for the computation of wind turbines (suggestion by Anonymous Reviewer #1)
- I formulated the purpose of the paper more precisely (requested by Anonymous Reviewer #1)
- I added a description of different gust modelling approaches in U-RANS solvers (suggestion by Anonymous Reviewer #1)
- I now distinguish between U-RANS and LES (suggestion by Anonymous Reviewer #1)
- I extended the description of the flow solver and the solver settings during the computation (suggestion by Anonymous Reviewer #1 and #2)
- I added a description of FAST which is needed for the validation (requested by Anonymous Reviewer #1)
- I added a description of the tower grid (requested by Anonymous Reviewer #2)
- I changed the text in section 3.2 to match the changes in figure 1
- I added a computation of the turbulence level in the $1 - \cos()$-gust case and gave a reason for the choice (suggestion by Anonymous Reviewer #1 and #2)
- I explained the oscillations in rotor thrust and rotor torque in figure 3,4 (suggestion by Anonymous Reviewer #1)
- I commented on the symmetric response to the gust in connection with the modelling assumption (suggestion by Anonymous Reviewer #1)
- I added a comparison between the THETA computation and FAST for validation (suggestion by Anonymous Reviewer #1)
- I added a description of the newly introduced figure 7 and clarified the information about the blade position of the investigated time instances (requested by Anonymous Reviewer #2)
- I added a comment about the link between rotor loading and vortex transport (suggestion by Anonymous Reviewer #1)
- I reflected on the dependence of infinite speed of sound and vortex transport in the case of changing wind speed (suggestion by Anonymous Reviewer #2)
- I deleted the description of figure 14 (suggestion by Anonymous Reviewer #2)

- I added a discussion for the newly introduced figures 12, 13. This implies a reduction of the discussion of the former figure 13, now figure 11 (suggested by Anonymous Reviewer #2)
- I changed the conclusion to match the changes in the paper.

Modifications of Figures

- I enlarged the figures
- I modified figure 1, to better represent the grid resolution
- I modified figure 5 to additionally include the validation with FAST
- I introduced figure 7 to display the span-wise distribution of rotor thrust and rotor torque (suggestion by Anonymous Reviewer #2)
- I summarized figures 7 to 11 to figure 8-10 to clarify the results (requested by Anonymous Reviewer #1 and #2)
- I changed the colour maps of figure 13 (now 11) (suggestion by Anonymous Reviewer #2)
- I deleted figure 14. Instead I entered 2 figures which are better suited to forward the discussion of vortex transport. (suggestion by Anonymous Reviewer #2)

Simulation of transient gusts on the NREL5 MW wind turbine using ~~CFD~~the U-RANS-solver THETA

Annika Länger-Möller[1]

[1]DLR Braunschweig; Lilienthalplatz 7; 38108 Braunschweig

Correspondence to: Annika Länger (annika.laenger@dlr.de)

Abstract. ~~The performed work presents a procedure , implemented in the CFD-solver THETA,~~ A procedure to propagate longitudinal transient gusts through a flow field by using ~~a resolved gust approach~~ the resolved-gust approach is implemented in the U-RANS solver THETA. Both, the gust strike of a $1-\cos()$-gust and an extreme operating gust following the IEC 61400-1 standard are investigated, on the generic NREL 5MW wind turbine at rated operating conditions~~are investigated with CFD~~. The impact of both gusts on pressure distributions, rotor thrust, rotor torque, and flow states on the blade are examined and quantified. The flow states on the rotor blade before the gust strike at maximum and minimum gust velocity are compared. An increased blade loading is detectable in the pressure coefficients and integrated blade loads. The friction force coefficients indicate the dynamic separation and re-attachment of the flow during the gust. Moreover, a validation of the method is performed by comparing the rotor torque during the extreme operating gust to results of FAST rotor code.

1 Introduction

The origins of applying Computational Fluid Dynamics (CFD) to wind turbine rotors date back to the 1990^{th} when Soerensen and Hansen (applied ElliSys3D to a wind turbine. Soerensen and Hansen (1998) solved the Reynolds Averaged Navier-Stokes (RANS) equations and applied the Menter SST $k-\omega$-turbulence model to a full scale wind turbine. In 2002 the National Renewable Energy Laboratory (NREL) performed an Unsteady Aerodynamic Experiment (UAE) (Hand et al., 2001) which has long been the reference for several CFD computations. For example, Johansen et al. (2002) presented a Detached Eddy Simulation (DES) on the NREL UAE phase VI blade to demonstrate the capabilities of predicting flow separation. Soerensen and Schreck developed a delayed DES to investigate whether the simulation approach could be improved. Furthermore, the experiment has been widely used for U-RANS solver validation for example by Duque et al. (2003); Le Pape and Lecanu (2004); Yelmule and Anjuri (201 .

Jonkman et al. (2009) developed the generic NREL 5MW wind turbine. Through its open access documentation, the NREL

5MW wind turbine is established as reference and validation test case for single- and multi physic test cases. For example, Chow and van Dam (2012) focused on the prediction of aerodynamic features of the wind turbine. Furthermore, they investigated the impact of fences on the flow separation in the inboard region. Full aero-elastic computations were performed by Bazilevs et al. (2011) for an isolated rotor and Hsu and Bazilevs (2012) respecting also the tower and nacelle. Bazilevs et al. (2011) and Hsu and Bazilevs (2012) modelled the aerodynamics with an U-RANS method and the structure with shell elements. The structure properties represented the material properties of the blade. The resulting aerodynamic characteristics and blade tip deflections were good when compared to the NREL 5MW documentation and FAST.

In the past years, the growing computer power enabled the geometry resolved simulation of wind turbines including the sites with Computational Fluid Dynamics (CFD). Studies have been performed for example by Schulz et al. (2016) or Murali and Rajagopalan (2017) who used an Unsteady Reynolds-Averaged Navier Stokes (U-RANS) solver to perform according studies. Moreover, hybrid Large Eddy Simulation(LES)-RANS approaches are implemented to analyse the behaviour of wind turbines in a complex terrain as for example presented by Castellani et al. (2017) who also considered the unsteady atmospheric inflow conditions.

The challenges of correctly predicting uncertainty of the fluctuating wind loads is a research field on its own. For example, Bierbooms and Drag (1999) or Suomi et al. (2013) investigated wind fields to better understand the shape of wind gusts. Matthäus et al. (2017) argued that a detailed understanding of wind fields is not necessary. Matthäus et al. rather respected unknowns of all parts of the wind turbine life cycle as for example changes in the blade shape due to production tolerances, ageing, or the wind field and summarized them in uncertainty parameters to estimate the effective power outcome and rotor loads. Mücke et al. (2011) proved that turbulent wind fields are not distributed Gaussian as assumed in the International Electrotechnical Commission Standard (IEC 61400-1). A similar conclusion was drawn by Graf et al. (2017) who investigated whether the 50 year loads as defined in the IEC 61400-1 adequately fulfil their purpose by applying different approaches of probability prediction to the generic NREL 5 MW turbine using the FAST rotor code.

The aerodynamic interferences between the unsteady wind conditions and wind turbines are of major importance for the prediction of fatigue loads and the annual power production. Therefore, it is part of the certification computation for each wind turbine. Nevertheless, the detailed investigation of isolated effects as the 50 year Extreme Operating Gust (EOG) on the flow of a wind turbine using high fidelity methods as CFD is rare even though the blade loads resulting from the extreme load cases are dimensioning load cases. In the case of vertical axis wind turbines Scheurich and Brown (2013) analysed the power loss of a wind turbine subjected to a sinusoidal fluctuation in wind speed. However, compared to the EOG amplitudes were small . Horizontal axis wind turbines which are hit by an EOG as defined in the IEC 61400-1 were presented by Sezer-Uzol and Uzol (2013). The wind turbine under consideration was the NREL phase VI rotor with a wind speed of $7\,\mathrm{m/s}$ using the panel code AeroSIM+. The impact of the gust was then evaluated ~~regarding~~ in terms of rotor thrust, torque and wake development. Preceding this study, Bierbooms (2005) examined the flap moment of wind turbine blades which were subjected to a gust with extreme raise~~in 2005, also using CFD.~~, using the wind turbine design tool Bladed. Bladed is an aero-elastic software by Garrad Hassan for the industrial design and certification of wind turbines (DNVGL, 2017). Other examples of aero-elastic simulation tools for wind turbine design are HAWC2 (Larsen and Hansen, 2015) or FAST (Sprague et al., 2015) which all include at least

a blade element momentum (BEM) method to represent the aerodynamics, a multi-body dynamics formulation to represent the structure, and an algorithm for rotational speed control. All three of them provide a possibility to compute EOG cases fully-multidisciplinary on the basis of linearized aerodynamic and structure models.

Even though the literature on gust simulations on wind turbines is rare, some research has been conducted in the field of aerospace science. Kelleners and Heinrich (2015) and Reimer et al. (2015) presented two approaches which are implemented in the U-RANS solver TAU (Schwamborn et al., 2006) to apply vertical gusts on airplanes: the velocity-disturbance approach and the resolved-gust approach ~~to apply vertical gust on airplanes~~. The velocity-disturbance approach adds the gust velocity to the surface of the investigated geometry . It enables the analysis of the resulting forces on the geometry surface but prevents the feedback of the structure response on the flow field and the gust shape. The resolved-gust approach overcomes the disadvantages of the one-way interaction in the velocity disturbance approach by propagating the gust through the flow field with the speed of sound. But it ignores that the gust transport-velocity usually differs from the speed of sound. The validity of both implementations was demonstrated by the time history of the position of the centre of gravity, pitch angles and load factors necessary for keeping the flight path of an aircraft constant.

In the so-called field approach Parameswaran and Baeder (1997) added the gust velocity to the grid velocity of the computational grid to all cells with

$$x \leq u \cdot t \tag{1}$$

wherein x is the coordinate in flow direction, u the transport velocity and t the physical time. This approach allows the definition of a gust transport-velocity and the analysis of the two-way interaction between gust, structure, and wake. Nevertheless, it requires a severe manipulation of the velocity field regardless of the flow solution that is produced by the wind turbine.

The simulation of unsteady inflow conditions of wind turbines in CFD implies several challenges: The simulation of a wind turbine including the tower is, itself, an instationary problem which needs the computation of several rotations to obtain a periodic solution. Superposed by ~~instationary~~ sheared inflow profiles and in-stationary (stochastic) inflow conditions, periodicity can never be gained because the same flow state never occurs twice. Moreover, a computation in which the rotor motion is adapted to the actual rotor forces using a strong coupling approach as proposed by Sobotta (2015) should be included in the computation. By using strong coupling between ~~CFD~~ the U-RANS solver Fluent and a pitch control algorithm for the rotor-motion Sobotta has been able to implement a simulation-procedure of turbine start-up. Heinz et al. (2016) performed the computation of an emergency shut-down of a turbine ~~also by using CFD~~ by using the incompressible U-RANS solver EllypSys3D and by neglecting the tower throughout the aerodynamic computations. Additionally, Heinz et al. considered the rotor mass and inertia by coupling of the ~~CFD~~ U-RANS solver with the aeroelastic code HAWC2.

The ~~present study aims for filling the gap in the gust simulation of wind turbines by applying~~ validation of the resolved-gust approach to DLR's U-RANS solver THETA ~~(Länger-Möller, 2017; Löwe et al., 2015). The generic NREL 5wind turbine at rated operating conditions is chosen as test case for~~ (Löwe et al., 2015; Länger-Möller, 2017) is presented herein. To reduce the complexity of the problem and emphasize the quality of the resolved gust approach, the NREL 5MW wind turbine is chosen to operate in shear-free conditions. Moreover, the possible interferences with the structure response and speed controllers are

reduced by using infinite rotor mass and inertia. Speed control algorithms are also neglected. As gust, a $1-\cos()$ shaped gust which lasts about 7 s and the EOG following the ~~international standard IEC 61400-1 definition. Rotor mass and inertia are set to infinity. Thus a computation respecting a pitch controller is not necessary, as the rotor will not accelerate during the gust strike. As results ,~~ IEC 61400-1 standard are chosen. As results rotor thrust and rotor torque, pressure distributions, friction force coefficients and the wake-vortex transport are evaluated. ~~To further simplify the evaluation of aerodynamic effects due to the gust, the atmospheric boundary layer is not considered during the study.~~ The rotor torque during the EOG is validated against FAST.

2 ~~Flow solver THETA~~Numerical methods

2.1 Flow solver THETA

DLR's flow solver THETA is a finite volume method which solves the incompressible Navier-Stokes (NS) equation on unstructured grids. The grids can contain a mix of tetrahedrons, prisms, pyramids and ~~hexahedrons~~hexagons. The transport equations are formulated on dual cells, which are constructed around each point of the primary grid. Therefore, the method is cell-centred with respect to the dual grid. The transport equations are solved sequentially and implicitly. The Poisson equation which links velocity and pressure is either solved by the SIMPLE algorithm for stationary problems or the projection method for unsteady simulations. With the projection method the momentum equations are first solved with an approximated pressure field. The pressure field then is corrected with a Poisson equation to fulfil continuity. Pressure stabilization is used to avoid spurious oscillations caused by the collocated variable arrangement.

The technique of overlapping grids (Chimera) is used to couple fixed and moving grid blocks~~(Kessler and Löwe, 2014)~~. The method was developed by Pan and Damodaran (2002) for structured grids or Zhang et al. (2008) for unstructured grids for the application in incompressible flow problems. It has been implemented to THETA by Kessler and Löwe (2014). The interpolation between the different blocks at interior boundaries is integrated in the system of linear equations on all grid levels of the multi-grid solver leading to an implicit formulation across the blocks . This procedure was identified to be crucial for achieving fast convergence of the Poisson equation.

Implicit time-discretization schemes of first order (implicit Euler) or second order (Crank Nicolson, BDF) are implemented. The temporal schemes are global time stepping schemes. A variety of schemes from first order upwind up to second order linear or quadratic upwind or a central scheme and the low dissipation, low dispersion second order scheme (Löwe et al., 2015) are implemented. Throughout this study, the second order central scheme is used.

The THETA code provides a user interface for setting complex initial and boundary conditions using the related C functions. This guarantees a high flexibility on the definition of boundary conditions and a straightforward modelling of very specific test cases. For example, the functions enable the prescription of gusts at the inflow boundary condition which are then propagated through the flow field. Moreover, all physical models are separated from the basis code. Therefore, new physical models can be implemented without modification of the base code.~~The user-interface is used extensively in the present study to prescribe the gust profile at the inflow boundary.~~

For turbulence modelling the commonly used Spalart-Allmaras, $k-\epsilon$, $k-\omega$ or Menter-SST models are available. ~~In former studies by Länger-Möller (2017), the~~ Since the early U-RANS computations of wind turbines the Menter-SST ~~lead to very good results for wind energy applications. Hence, this~~ turbulence model is used (Soerensen and Hansen, 1998) for wind turbine applications. Recently, Länger-Möller (2017) confirmed this finding during the THETA validation by comparing the results of common one- and two equation turbulence models to the NREL UAE phase VI experiment. Hence, the Menter SST turbulence model is applied throughout the present study. ~~The time step~~ Moreover, according to the studies in Länger-Möller (2017) a time step of $\delta t = 0.006887052\,\mathrm{s}$ which is equivalent to a rotor advance of $\Psi = 0.5°$ is chosen . As time stepping scheme, the Eulerian implicit scheme for the temporal discretization is chosen. To ensure convergence in every time step, a residual of less than 10^{-5} has to be reached. Moreover, the solver has to perform at least 20 iterations per time step in all equations. Due to efficiency reasons, the maximum number of iterations per time step is limited to 100.

2.2 FAST

The comprehensive rotor code FAST (Sprague et al., 2015) is a modular software framework for computer aided engineering (CAE) of wind turbines. FAST provides a coupling procedure to compute time-dependent multi-physics relevant for wind turbine design. By the means of different modules, FAST is able to respect different physical models and turbine components in the computations. The aerodynamics are represented by a blade element momentum method (BEM) which is based on profile polars for drag, lift and momentum.

In the present case, the variable-speed control was turned off to ensure a constant rotational speed as in the U-RANS computation. The blade stiffness has been increased to the order of $10^{29}\,\mathrm{Nm}^2$ per blade element to obtain a stiff blade.

To ensure a shear-free inflow profile, the the constant wind profile type was selected. In FAST, the EOG started after the computation of $8\,\mathrm{s}$. The analytical inflow profile was included as x-velocity in the IECWind file. The other wind directions were equal to 0.

3 Geometry

3.1 NREL 5MW wind turbine

The NREL 5MW turbine (Jonkman et al., 2009) is a three bladed wind turbine with a rotor radius of $63.0\,\mathrm{m}$ and a hub height of $90\,\mathrm{m}$. The rotor has a cut-in wind speed of $v_{ci} = 3\,\mathrm{m/s}$ and a rated wind speed of $v_{rated} = 11.4\,\mathrm{m/s}$. Cut-in and rated rotational speeds are $\omega_{ci} = 41.4\,°/\mathrm{s}$ and $\omega_{rated} = 72.6\,°/\mathrm{s}$, respectively. The blades are pre-coned and the rotor plane is tilted about $\beta = 5.0°$ and not yawed. Along the non-linearly twisted blade 7 different open-access profiles are used.~~For detailed information please refer to Jonkman et al. (2009).~~

Due to ~~meshing issues the nacelle~~ the narrow gap between rotor and nacelle a valid chimera overlap-region could not be achieved in that region. Thus the nacelle of the NREL 5MW turbine is neglected while the tower is respected. This approach leads to an error in the flow prediction behind the rotor hub but is supposed to have no impact on the blade loads.

The gust simulation is based on the rated wind speed $v_{rated} = 11.4\,\mathrm{m/s}$. Air density of $\rho = 1.225\,\mathrm{kg/m^3}$ and the kinematic viscosity of $\nu = 1.82 \cdot 10^{-5}\,\mathrm{m^2/s}$ is used. To isolate the gust impact of the rotor loads, a shear-free velocity profile is considered throughout the computation.

3.2 Grid characteristics

The computational grid consists of 3 parts. The first part contains the three rotor blades, stubs and the rotor hub. On the blade surface, a structured grid with 156×189 elements in span-wise and chord-wise direction was generated. The boundary layer mesh of the blades consists of 49 ~~hexahedra~~ hexagon layers in an O-O-topology. The height of the wall-next cell is $\delta = 3 \cdot 10^{-6}\,\mathrm{m}$ along the entire blade, ensuring $y^+ \leq 1$. Figure 1a) and b) gives an impression of the chord-wise and span-wise grid resolution, respectively.

The second part of the grid has the shape of a disk and contains the entire rotor. The disk measures $D = 166.7\,\mathrm{m}$ in diameter and has a depth of $26.7\,\mathrm{m}$. It is filled with tetrahedrons with an edge length between $0.002\,\mathrm{m}$ and $0.9\,\mathrm{m}$. The entire disk is used as chimera child grid for the overlapping grid technique and contains approximately $11.63 \cdot 10^6$ points.~~The disk is displayed in figure 1(a) wherein the black coloured blade number 1 is at zero-azimuth position ($\Psi = 0$).~~

The chimera parent grid has the dimensions of $504 \times 504 \times 1512\,\mathrm{m^3}$ in width, height, and length. It contains a boundary layer grid of the floor, the tower, and a refined grid region to resolve the rotor wake up to $3R$ downstream.

The 54 prism layers, used to resolve the boundary layer of the viscous floor, have a total height of $H = 5\,\mathrm{m}$ with a wall-next cell height of $\delta = 3 \cdot 10^{-5}\,\mathrm{m}$. The floor is defined as viscous wall. This meshing strategy enables the comparison of future gust computations that include sheared inflow profiles. The tower surface grid is meshed structured in a height below $5\,\mathrm{m}$ with 54 point in height and 180 points in radial direction. Above $5\,\mathrm{m}$, a triangulated unstructured grid is generated with the maximum edge length of $0.55\,\mathrm{m}$. As the tower surface is modelled as slip-wall, tetrahedrons are built directly on the tower surface.

In the chimera parent grid, the edge length of the cells continuously grow from very small in the rotor-tower and wake region to rather large close to the farfield boundaries. The entire chimera parent grid contains approximately $13.25 \cdot 10^6$ points.

In figure 1c) the entire chimera setup is displayed and the boundary conditions are indicated. The upwind and downwind boundaries are defined as inflow and outflow respectively. At the inflow boundary surface, the turbulence quantities and inflow velocities are prescribed. Later, also the gust profile is introduced in this boundary. The floor is defined as viscous wall~~and the remaining farfield surface is defined as no-slip wall.~~ . The surfaces on top, left and right of the flow domain are defined as slip wall.

4 Gust modelling

4.1 The resolved-gust approach

The procedure of applying the gust to the flow field starts by computing the flow field around the wind turbine ~~in question~~ until the flow field and the global rotor loads have become periodic. For the NREL 5MW turbine in the given setup 9 revolutions are

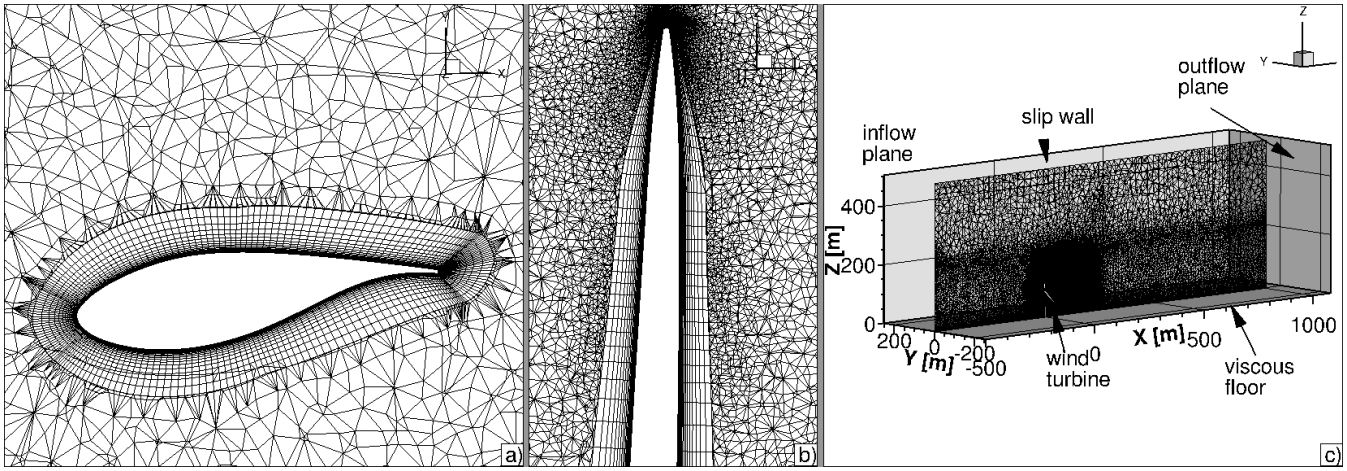

Figure 1. Computational grid setup; a) Chord wise distribution; b) span wise distribution in blade tip region; c) Cut through the flow field and boundary conditions

required. Then, the inflow velocity on the inflow boundary is modified according to the velocity change described in section 4.2 or 4.3. The computation is continued so that the gust is propagated through the flow field. In the approach by Kelleners and Heinrich (2015) and Reimer et al. (2015) using ~~CFD~~ TAU (Schwamborn et al., 2006) to solve the compressible RANS equations, the gust is transported with the speed of sound. In their approach, as well as in the present paper, the computation has been run at least until the gust has entirely passed the geometry in question but can be continued as long as wished by the user.

The restrictions ~~on the resolved-gust approach named by Kelleners and Heinrich (2015) and Reimer et al. (2015)~~ to ensure a loss-free transport of the gust velocity on the resolved-gust approach named by Kelleners and Heinrich (2015) or Reimer et al. (2015) are

- a fine grid upstream of the geometry in question
- a fine time step.

As THETA is an incompressible solver, the speed of sound is infinite. In addition to the strong implicit formulation and the choice of boundary conditions that prevent the flow from escaping sideways, this leads to a spread of the gust velocity through the flow field instantaneously. If the same gust velocity is added to the constant inflow condition in every point in the inflow plane and the boundary conditions are chosen as specified in section 3.2, the transport of the gust velocity will be loss-free through the entire domain. Hence, the restrictions by Kelleners and Heinrich (2015) and Reimer et al. (2015) ~~regarding~~ concerning the grid resolutions are obsolete while a fine time step is required to ensure numerical stability.

To analyse the resolved gust approach in the incompressible U-RANS solver THETA, the inflow velocity profile is shear-free and the gust velocity remains independent of the height above ground.

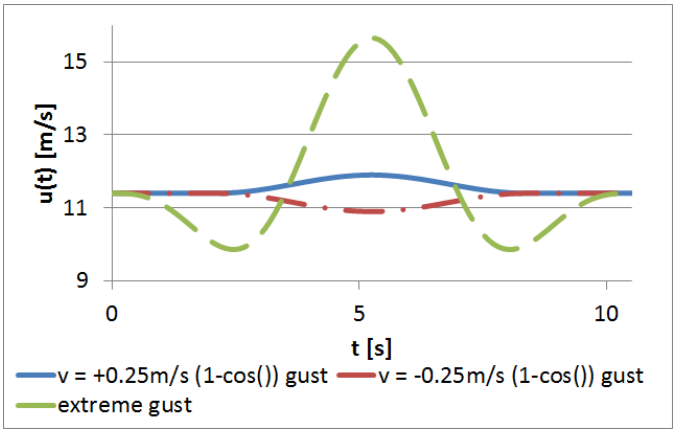

Figure 2. Inflow velocity in dependence of physical time t

4.2 Cosines gust

The $1-\cos()$ gust is modelled in analogy to the EASA certification standard (EASA, 2010) as

$$u(t) = u_g \left(1 - \cos\left(\frac{8\pi}{H}\right)\right) \tag{2}$$

with $u(t)$ and u_g as the time dependent velocity and the gust velocity, respectively and H as gust gradient. In the work presented, H is ~~defined as~~ chosen to generate a non-compressed sinusoidal gust

$$H = \frac{8\pi}{t - T_S} \tag{3}$$

wherein t represents the actual physical time and T_S is the time at which the gust ~~started~~starts. Inserting equation 3 in equation 2 the following definition of the gust results:

$$u(t) = \begin{cases} u_g(1 - \cos(t - T_S)) & \text{if } T_S \leq t < T_S + T_g \\ u & \text{if } t \leq T_S \text{ or } t \geq T_S + T_g \end{cases} \tag{4}$$

Wherein T_g is the duration time of the gust. The gust velocity u_g is defined as $+0.25\,\mathrm{m/s}$ representing a gust and $-0.25\,\mathrm{m/s}$ representing a sudden calm. In both cases, the maximum change in wind speed is $0.5\,\mathrm{m/s}$ or $4.4\,\%$ at rated wind speed of the NREL 5MW turbine. The ~~resulting inflow velocities are~~ turbulence intensity of the $1-\cos()$-gust is $2.5\,\%$ which is in the order of the atmospheric turbulence intensity that Schaffarczyk et al. (2017) found in a field measurement campaign on a horizontal wind turbine. The resulting gust profile of the present study is displayed in figure 2.

4.3 Extreme operating gust

The time dependent velocity change of the ~~extreme gust is modelled with IEC 61400-1 2005~~ EOG is modelled following the IEC 61400-1 standard.

$$u(z,t) = u(z) - 0.37 \cdot u_g \sin\left(\frac{3\pi \cdot t}{T_g}\right) \cdot \left(1 - \cos\left(\frac{2\pi \cdot t}{T_g}\right)\right). \tag{5}$$

Wherein $T_g = 10.5\,\mathrm{s}$ is the ~~gust characteristic time~~ characteristic time as defined in the IEC 61400-1 (2005), t the computational time, $u(z)$ the velocity profile depending on the height and ~~the gust speed~~ the gust velocity. The latter is defined as

$$u_g = 3.3 \left(\frac{\sigma_1}{1 + 0.1\left(\frac{D}{\lambda_1}\right)}\right) \tag{6}$$

and is $5.74\,\mathrm{m/s}$ in the given case. In equation 4, $\sigma_1 = 0.11 \cdot v_{hub}$ is the standard turbulence deviation, $\lambda_1 = 42\,\mathrm{m}$ the turbulence scale parameter and D the rotor diameter. u_{hub} represents the velocity at hub height. The velocity u_{e1} is the average over 10 minutes with a recurrence period of 1 year. It is defined as

$$u_{e1} = 1.12 \cdot u_{ref} \left(\frac{z}{z_{hub}}\right)^{0.11} \tag{7}$$

with the reference velocity $v_{ref} = 50\,\mathrm{m/s}$. It is defined in the IEC 61400-1 standard for a wind turbine ~~for the A1 wind class . By respecting a height-independent flow profile, evaluating equation 6 for the given flow conditions and~~ of the wind class A1. In a shear-free inflow, the inflow velocity is constant with height and thus $u(z)$ reduces to u and $u(z,t)$ to $u(t)$. By additionally entering equation 7 in equation 5 one obtains the final gust definition

$$u(t) = u - 0.37 \cdot u_g \sin\left(\frac{3\pi \cdot t}{T_g}\right) \cdot \left(1 - \cos\left(\frac{2\pi \cdot t}{T_g}\right)\right). \tag{8}$$

The resulting gust profiles of the EOG in comparison to the moderate $1 - \cos()$-gust is visualized in figure 2.

5 Results

5.1 Constant inflow conditions

As described in section 4.1 a periodic flow field with periodic rotor loads is mandatory as ~~initial~~ starting conditions for computing gusts that act on wind turbines. The resulting time history of rotor thrust F_x and rotor torque M_x for constant inflow conditions over revolution 6 to 10 are displayed in figures 3 and 4 with the red line. In both figures the periodic behaviour of a periodic flow field is visible as well as the typical $3/rev$-characteristic of a rotor-tower configuration of the wind turbine. ~~The average value of~~ By averaging rotor thrust F_x and torque M_x ~~over the four revolutionsdisplayed is~~ about 4 revolutions, one obtains $738.9\,\mathrm{N}$ and $4.15\,\mathrm{MNm}$, respectively. Compared to the reference of Jonkman et al. (2009) ~~, rotor thrust and torque~~ at rated conditions the values deviate about approximately $-3.77\,\%$ and $-0.98\,\%$, respectively. Imiela et al. (2015) achieved a

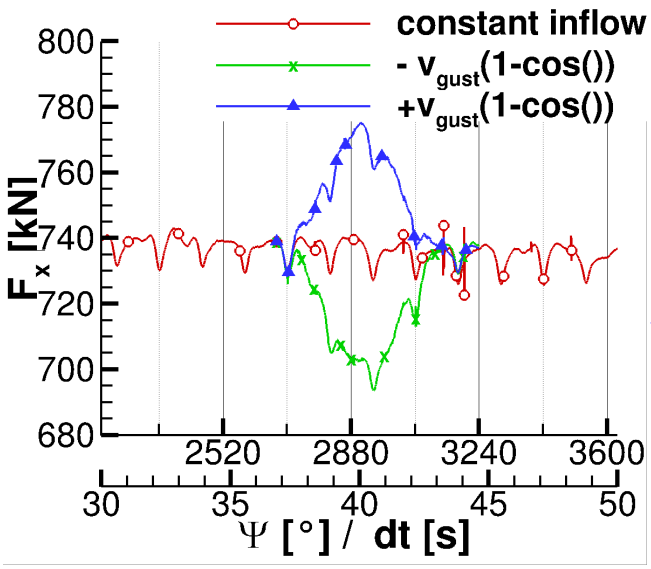

Figure 3. Rotor thrust F_x during the gust

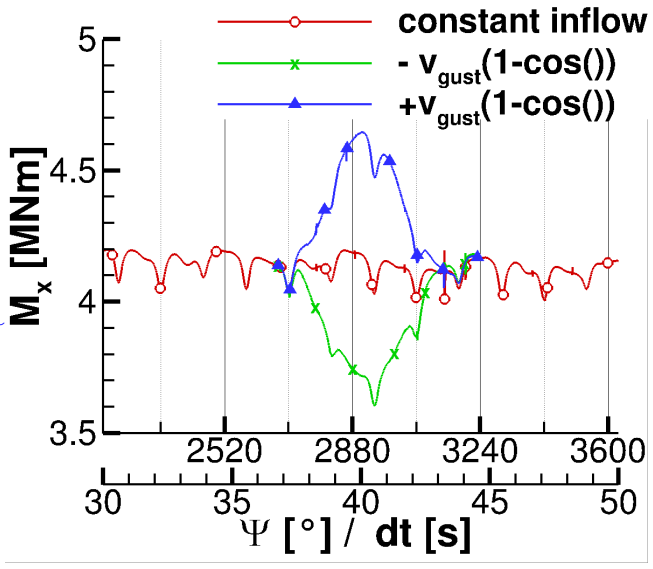

Figure 4. Rotor torque M_x during the gust

rotor thrust of 786 kN and a torque of 4.4 MNm in their studies with the compressible U-RANS solver TAU for the stiff-bladed NREL 5MW turbine.

The agreement between the ~~CFD computation~~ U-RANS computations performed with THETA, TAU and the ~~values obtained with linearised models which were used to generate~~ reference documentation of the NREL 5MW ~~documentation~~ wind turbine (Jonkman et al., 2009) is excellent. Thus, the numerical setup is validated successfully.

Between $\Psi = 3060°$ and $\Psi = 3240°$, in the 8^{th} revolution, high-frequency oscillations occur in the THETA computation. In the specific time step, the Poisson equation for pressure correction has not converged in the maximum number of iterations. Nevertheless, the interference subsides in the following rotor rotations and is sufficiently small. Thus, the reason for this oscillations is of minor importance in the context of this paper.

If the wind turbine operates in uniform flow conditions, a $3/rev$-characteristic is found in both F_x and M_x, which is caused by the tower blockage effect. Moreover, the constant amplitudes around a steady mean values of both, F_x and M_x indicate that the flow field has converged. Hence, the gust ~~can be applied~~ as defined in equation 4 or 8 are applied in the next step.

5.2 Cosines gust

The impact of the $1 - \cos()$- gust ~~is evaluated regarding~~ on rotor thrust F_x and rotor torque M_x during the gust is evaluated by comparison to uniform inflow conditions. F_x and M_x are displayed in figure 3 and 4, respectively. Therein, the period between 30 s and 50 s is displayed while the gust operates between $T_S = 37$ s and $T_S + T_g = 44$ s. Thus, it lasts approximately 1.5 rotor revolutions. As expected, the gust velocity spreads over the entire field immediately and also affects rotor thrust and rotor torque instantaneously. In the case of gust and calm no hysteresis effect is found as rotor thrust and rotor torque recover

Table 1. Gust induced peak loads on the rotor during the $1-\cos()$-gust in relation to the constant ~~averaged~~ blade load

	δF_x [%]	δM_x [%]
$u_g = +0.25\,\mathrm{m/s}$	+5.6	+12.9
$u_g = -0.25\,\mathrm{m/s}$	-5.6	-12.4

Table 2. Averaged rotor loads during the $1-\cos()$-gust in relation to the constant ~~averaged~~ blade load

	$\delta\overline{F_x}$ [%]	$\delta\overline{M_x}$ [%]
$u_g = +0.25\,\mathrm{m/s}$	+2.4	+5.7
$u_g = -0.25\,\mathrm{m/s}$	-2.1	-4.6

immediately after the gust. This is visible in both figures 3 and 4 as the curve of constant inflow conditions is matched right after $44\,\mathrm{s}$. The symmetric response of rotor thrust and rotor torque to the gust is caused by the modelling assumptions of a stiff blade and a missing speed control algorithm.

During the gust, F_x and M_x follow the modification of the inflow condition. Hence, for a positive gust velocity u_g (equation 4) rotor loads increase in a $1-\cos()$-shape while they decrease in the same manner for a negative gust velocity. Additionally, the tower blockage effect is superposed on the blade loads and remains detectable in the blade load development. ~~Furthermore~~In the case of $u_g = +0.25\,\mathrm{m/s}$, the tower blockage effect reduces the time that the rotor experiences maximum loads ~~in the case of $u_g = +0.25\,\mathrm{m/s}$,~~ as is visible at approximately $t = 41\,\mathrm{s}$. A sharp drop in both, rotor thrust and rotor torque, is visible. This drop is due to the tower blockage effect and would have appeared at a different ~~time~~ instance of the gust if the rotor position at the gust starting time was different. Nevertheless, during the calm with $u_g = -0.25\,\mathrm{m/s}$ the tower blockage leads to an additional decrease in rotor thrust and rotor torque at $t = 41\,\mathrm{s}$. The rapid changes in rotor thrust and rotor torque indicate the fast load changes on the blade which ~~would~~ increase fatigue loads.

Table 1 lists the relative differences in F_x and M_x during the gust, computed ~~following~~ by equation 9. In equation 9 the subscript max indicates the extreme rotor loads and the over-line the ~~average of~~ averaged rotor loads under constant inflow conditions ~~over 4 revolutions~~ of section 5.1

$$\begin{aligned}\delta F_x =& 100 \cdot \left(\frac{F_{max}}{\overline{F_x}} - 1\right)\\ \delta M_x =& 100 \cdot \left(\frac{M_{max}}{\overline{M_x}} - 1\right).\end{aligned} \tag{9}$$

Additionally, the relative difference in the averaged blade load is computed by first integrating rotor thrust and rotor torque during the gust excitation and then computing equation 9. The result of the gust peak load is listed in table1 while the integrated loads are contained by table 2.

In both tables it can be seen that a reduction of the wind ~~velocity~~ speed due to a calm or the increase of the wind ~~velocity~~ speed with the same amplitude leads to ~~almost identical~~ very similar absolute changes in rotor thrust and ~~torque.~~rotor torque.

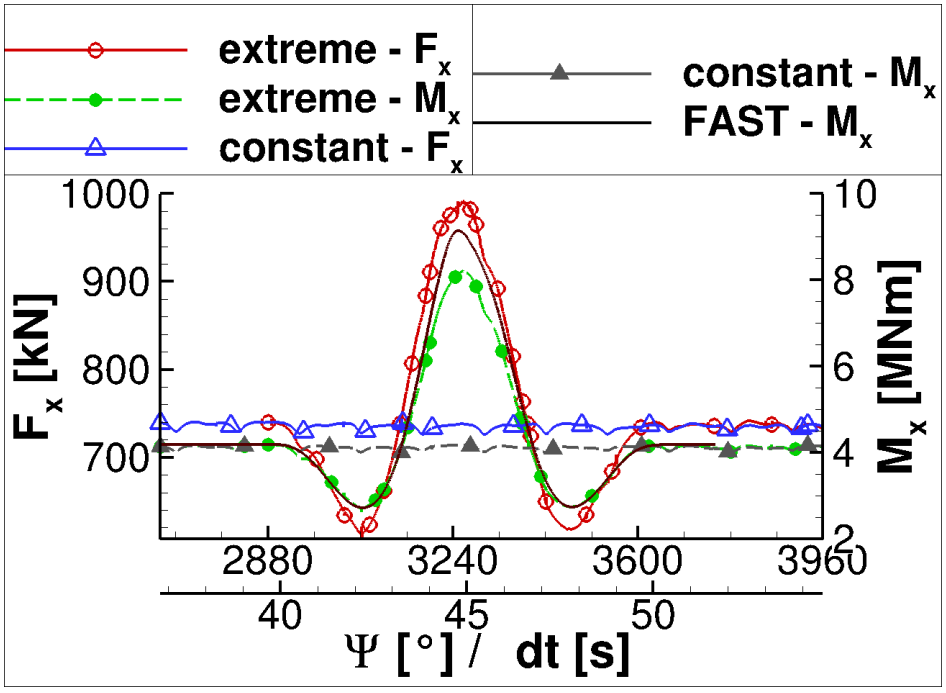

Figure 5. Rotor thrust F_x and torque M_x during the gust

By comparing the values of table 1 and 2 it is also found that the absolute peak loads are 2.3 times larger than the averaged loads. Thus, the use of maximum loads during a 10 min-interval is inevitable for a computation of equivalent fatigue loads while averaging the loads is not appropriate.

It is also important to note that the rotor loads return to the values of constant inflow conditions right after the gust ended. This indicates that there are ~~no reflections or~~ neither reflections nor numerical oscillations in the flow field which lower the numerical accuracy. In summary, the behaviour of rotor thrust F_x and rotor torque M_x is as expected. The increased wind ~~velocity~~ speed causes higher thrust and momentum and vice versa while the amplitude is identical for the increase and decrease in wind ~~velocity~~speed.

By considering blade deflections and changes to the rotational speed in future aero-elastic computations, the resulting rotor torque and rotor thrust will change.

5.3 Extreme operating gust

Figure 5 presents rotor thrust F_x and rotor torque M_x ~~are presented during the extreme gust excitation and~~ during the EOG excitation in comparison to the constant inflow conditions. ~~The extreme gust~~ Moreover, the rotor torque that is computed by FAST for a stiff blade and constant rotational speed is displayed. The EOG lasts about 10.5 s or 2 rotor revolutions. In comparison to the rotor loading during the ~~gust, described in section 5.2,~~ $1 - \cos()$-gust (section 5.2) the tower blockage effect

Table 3. Gust induced peak load during the EOG on rotor in relation to the constant ~~average~~ blade load

	δu [%]	δF_x [%]	δM_x [%]
$u_g(min)$	-13	-17.3	-36.0
$u_g(max)$	$+37$	$+35.0$	$+100.2$

becomes negligible. Hence, the starting position of the rotor is less important for the computation of maximum loads. This is also seen in the FAST result. By comparing the rotor torque during the gust of THETA to the one of FAST it is found that both values coincide exactly before $t = 43.5\,\mathrm{s}$ and after $t = 46.5\,\mathrm{s}$. Between this two time stamps, FAST predicts significantly higher loads than THETA. Moreover, the EOG load at the maximum gust velocity is increased in comparison to THETA. The differences result from the flow characteristics of the blade. THETA predicts large areas of flow separation as response to accelerated velocity after $t = 43.5\,\mathrm{s}$. The flow reattaches over most of the blade after $t = 46.5\,\mathrm{s}$ when the velocity slowed down sufficiently. It is most likely that the profile polars that the BEM of FAST relies on is not able to reproduce the instationary flow behaviour of the given case.

The maximum velocity u_{max} during the gust is about $15.65\,\mathrm{m/s}$ and the minimum velocity u_{min} is $9.94\,\mathrm{m/s}$ which are $137\,\%$ and $87\,\%$ of the values at rated wind speed. The changes in rotor thrust and rotor torque, computed by equation 9, are given in table 3. It is shown that the rotor torque is decreased by $36\,\%$ during the calm that precedes or follows the velocity ~~peak~~ maximum and increased about $100\,\%$ during the gust peak. The changes in rotor thrust are smaller even though the amplitudes of load change are significant as well.

~~Similar changes to those in rotor thrust and torque are, of course, also visible in pressure distributions and friction forces.~~ To analyse the flow state on the blade during the gust two instances have been chosen: after $t_{min} = 2.5s + T_S = 42\,\mathrm{s}$ (minimum gust velocity) and $t_{max} = 5.6s + T_S = 45\,\mathrm{s}$ (maximum gust velocity). Figure 6a) and b), respectively, display the rotor positions in the instances investigated. In both figures blade number 1 is coloured in black. At t_{min}, when the gust is at its minimum ~~speed~~velocity, blade number ~~one~~ 1 is right in front of the tower and additionally experiences the tower blockage effect. Conversely, at t_{max}, when the gust is at its maximum ~~speed~~velocity, blade number 1 is in free stream conditions while the flow on blade number 3 ~~is influenced by~~ enters the tower blockage ~~. For a meaningful comparison with pressure and friction coefficients from~~ region. The impact of the tower blockage during the constant inflow conditions ~~, it was ensured that the investigated sections result from blades at the same azimuth positions. The pressure distributions along with the friction forces are investigated~~ at t_{min} and t_{max} is visible in the radial distribution of rotor thrust and rotor torque (figure 7).

In accordance to figure 5 the overall rotor loading is reduced when the blade experiences minimum gust velocity. Conversely, a significant increase in rotor loading is observed when the blade experiences the maximum gust velocity. At all times, the rotor thrust is reduced only slightly by the tower blockage effect. Moreover, only the inboard part of the rotor appears to be affected by the tower blockage. Contrariwise, the rotor torque is affected by the tower blockage in the outer part of the rotor. Besides, the tower blockage effect generally has only small impact on the rotor torque at wind velocities smaller than rated wind speed. With the maximum gust velocity, the blade at $\Psi = 210°$ experiences a strong tower blockage effect that reduces

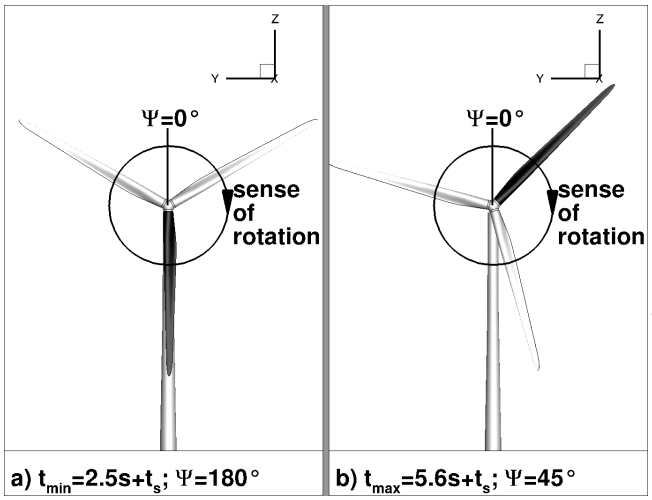

Figure 6. Rotor position at minimum (left) and maximum (right) gust velocity; Black blade is blade number 1

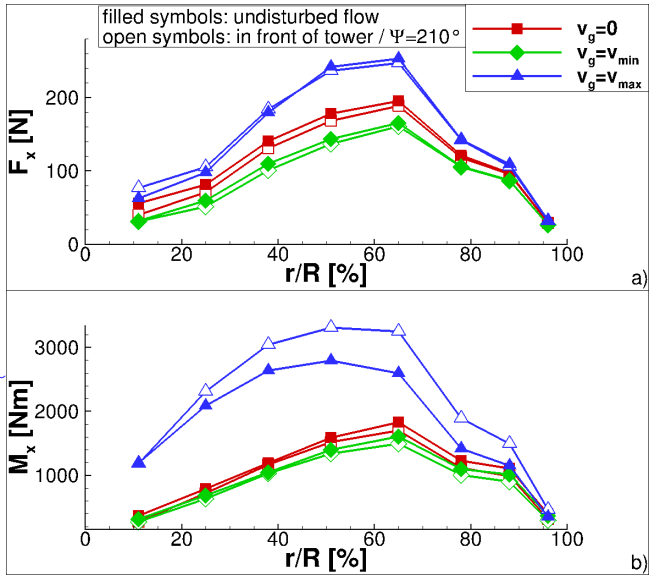

Figure 7. Span-wise distribution of a) rotor thrust and b) rotor torque for different azimuth positions at constant inflow and during the gust

the rotor torque up to 29% (radial section $r/R = 65\%$). The reason is the different separation behaviour at the trailing edge of the blade which are investigated through pressure coefficient distributions and friction force coefficients at three radial sections: an inboard section at $r/R = 10\,\%$, a mid-section $r/R = 50\,\%$ and an outboard section at $r/R = 90\,\%$. They are displayed in figure 8, 9 and 10, respectively.

In all three figures the pressure is displayed in the upper half and is normalized with the vector sum of the tip speed ~~velocity~~ and the constant inflow velocity. For a meaningful comparison to constant inflow conditions, it was ensured that the investigated sections result from blades at the same azimuth positions.

A noticeable difference in c_p at minimum gust velocity is found in all sections (figures 8a), 9a), and 10a)) when compared to the constant inflow conditions. The decrease in the stagnation point of c_p to lower values ~~due to the calm at $t_{min} = 42\,s$~~ at t_{min} is higher than that of the tower blockage effect while otherwise the pressure distributions keep the general shape. Conversely the difference between constant inflow conditions and the maximum gust is significantly higher. The maximum c_p increased about $58\,\%$ at the blade tip~~section~~. Moreover, the shape of the pressure distribution ~~is changed~~ changes over the entire blade. This is visible especially in the mid- and outboard blade sections (figures 9a) and 10a)). In both sections, the pressure increases rapidly in the rear half of the upper blade surface and even reaches positive values in the last $20\,\%$ of the profile. This behaviour is a first indication of a separation region and reversed flow around the trailing edge.

The ~~indications about separation that were made in the pressure distributions are enhanced by analysing the~~ friction coefficients on the blade ~~. The friction coefficients on the blade~~ sections in undisturbed flow are displayed in figures 8c), 9c), and 10c).

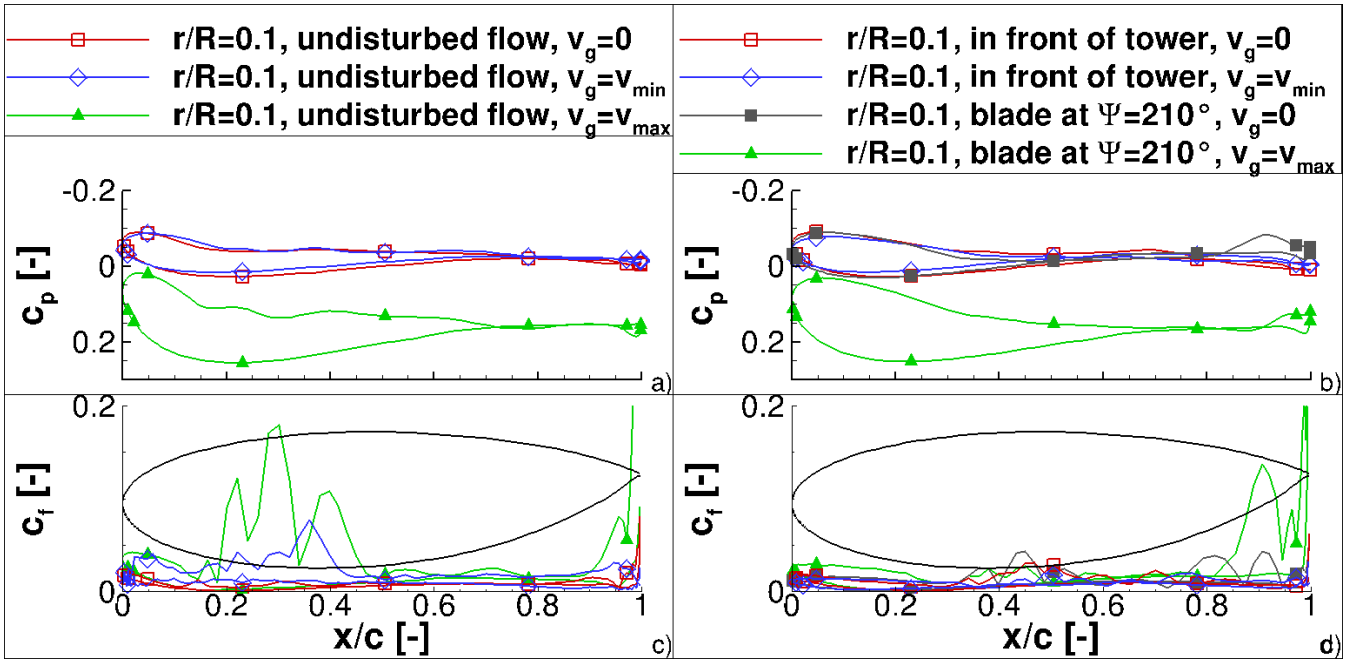

Figure 8. Pressure distribution of blade at inboard section; a,c) undisturbed flow; b,d) with tower blockage; a,b) pressure distribution, c,d) friction force coefficient

In all sections, strong fluctuations are visible at the trailing edge which result from the truncated geometry at $x/c = 1$. The friction force coefficient c_f in the inboard section (figure 8c)) shows large differences between all considered time instances. The oscillations around $x/c = 50\,\%$ at constant inflow conditions indicate a small separation region with otherwise attached flow. At minimum gust velocity the overall friction force level is increased around the leading edge and the separation region has shifted upward and is between $x/c = 20\,\%$ and $x/c = 40\,\%$. At the maximum gust velocity, the friction force is increased and the oscillations between $x/c = 20\,\%$ and $x/c = 50\,\%$ indicate a larger separation region on the upper blade surface. The friction force coefficient indicates that separation in the blade inboard section is present during the entire rotor rotation. It is triggered through the close cylindrical blade root and amplified with higher inflow velocities. Conversely to the inboard section, changes in separation at the mid-section appear due to the gust only. In figure 9c) the friction force level is decreased at minimum gust velocity and the curve is very smooth. At maximum gust velocity, small oscillations appear around $x/c = 90\,\%$, indicating separation in that region. By increasing the rotor radius, the behaviour is enforced. At the outboard section (figure 10c)), the local maximum in c_f in the last $20\,\%$ of the profile almost reaches the level of the leading edge ~~during the maximum gust velocity.~~ at t_{max}.

The same analysis ~~of pressure coefficients~~ is performed for the blade that is situated right in front of the tower or ~~in the influence of the tower blockage 30 ° before the tower. The according figures are displayed in figures~~ at $\Psi = 210\,°$. For the pressure distributions figures 8b), 9b), 10b)) the same effects as described for the blades in undisturbed flow are found. The only difference

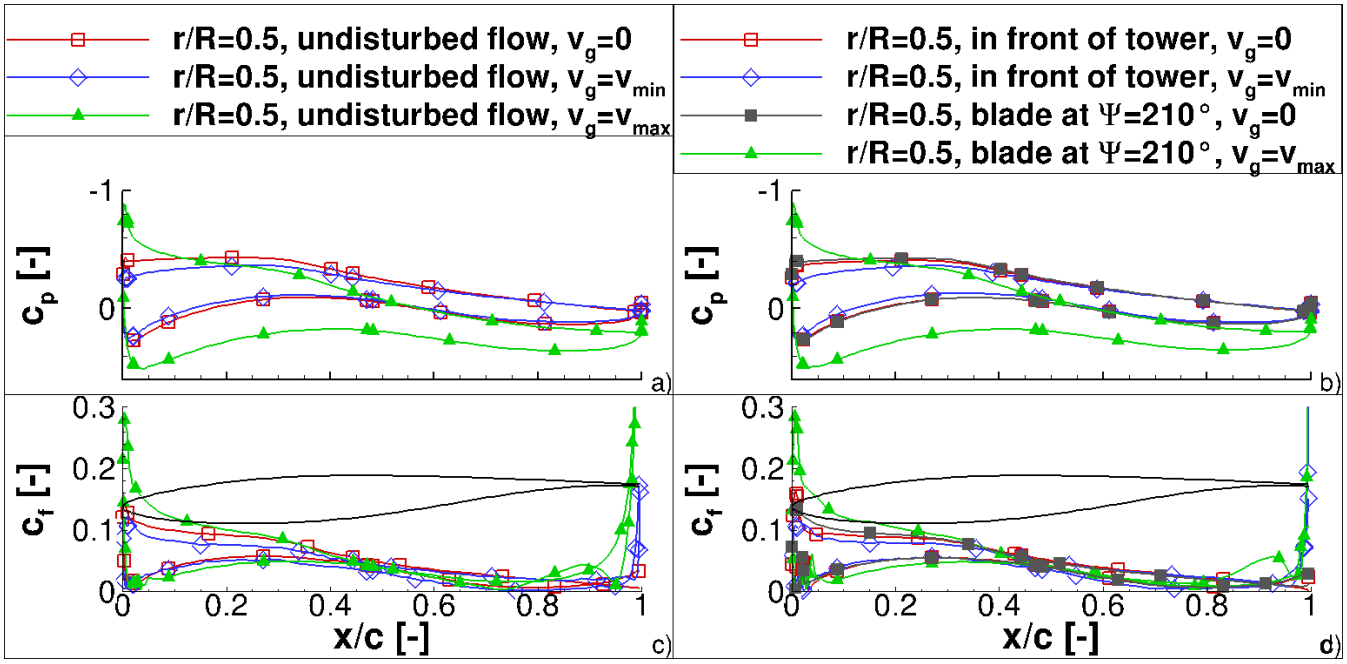

Figure 9. Pressure distribution of blade at mid section; a,c) undisturbed flow; b,d) with tower blockage; a,b) pressure distribution, c,d) friction force coefficient

is that due to the tower blockage the overall pressure level is decreased about ~~1,%.~~ 1 %. This enforces the observation from the rotor thrust and rotor torque time histories in figure 5 and 7. Namely, the tower blockage effect is small compared to the EOG operating loads. Conversely, the characteristics of friction forces (figures 8d), 9d), and 10d)) in the inboard and outboard sections differ from those of the blades in undisturbed flow. In the inboard section in figure 8d), the oscillations in c_f reduce to a minimum while the overall friction force level remains constant. Only at maximum gust velocity, ~~some fluctuations~~ the oscillations around the trailing edge appear. Thus, the tower seems to suppress separation and it takes some time until the separation state is fully recovered. The friction force coefficient in the mid-section behaves similar to the inboard section with the difference that the entire separation region is ~~increased~~ larger (figure 9d)). In the outboard section in figure 10d), the friction force is increased significantly due to the maximum gust velocity. By comparing the friction coefficients of the blades in undisturbed flow and in the tower blockage region, it is found that the separation on the suction side of the blade covers a larger area in the rear part of the blade. The separation induces a larger profile thickness which results to different induced angle of attack and thus reduced momentum.

Finally, the transport of the tip vortices is investigated. It has to be understood as indication whether the velocity transport in the field works as expected but the tip-vortex transport has only small meaning on the transient rotor loading during the gust. Besides, the velocity in the field changes gradually because of the infinite speed of sound in the entire flow domain. Thus, the vortices that are shed from the blade at a given wind speed are not transported with their specific transport velocity.

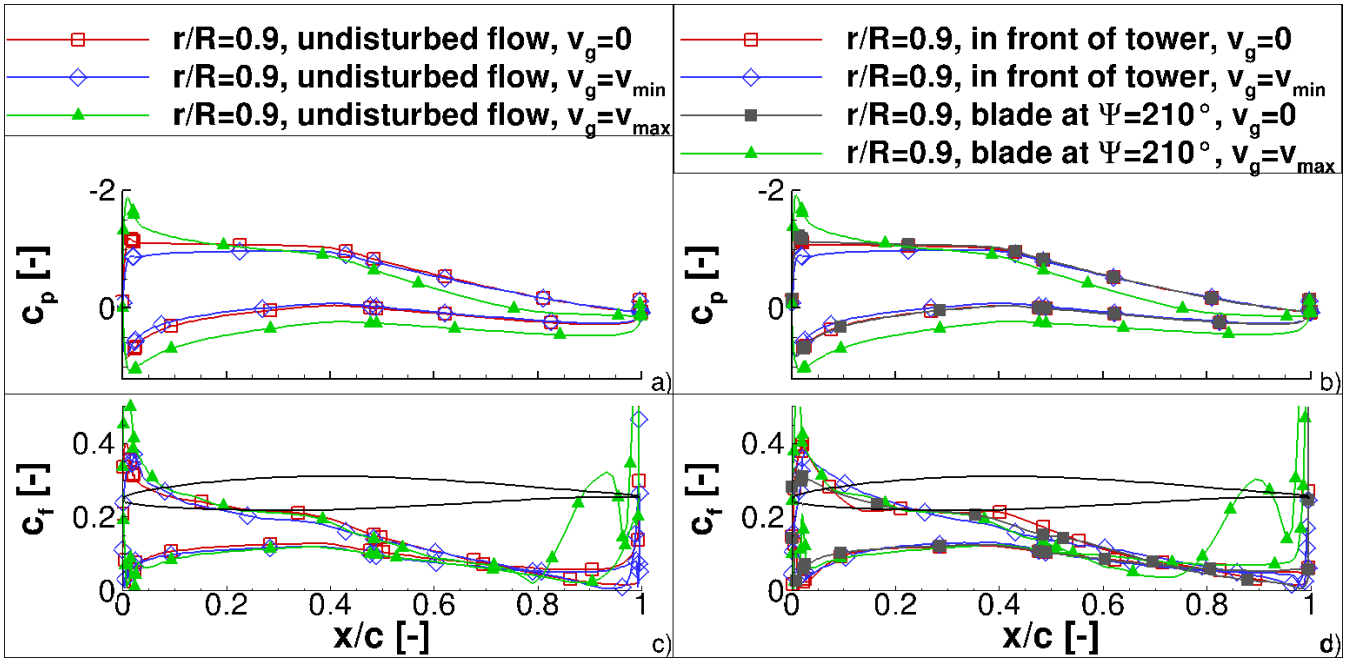

Figure 10. Pressure distribution of blade at outboard section; a,c) undisturbed flow; b,d) with tower blockage; a,b) pressure distribution, c,d) friction force coefficient

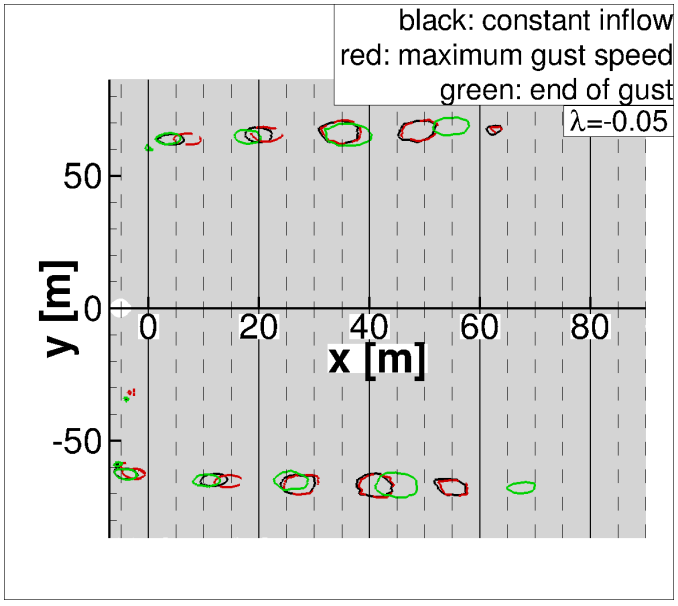

Figure 11. Tip vortex transportation in vertical plane through rotor centre

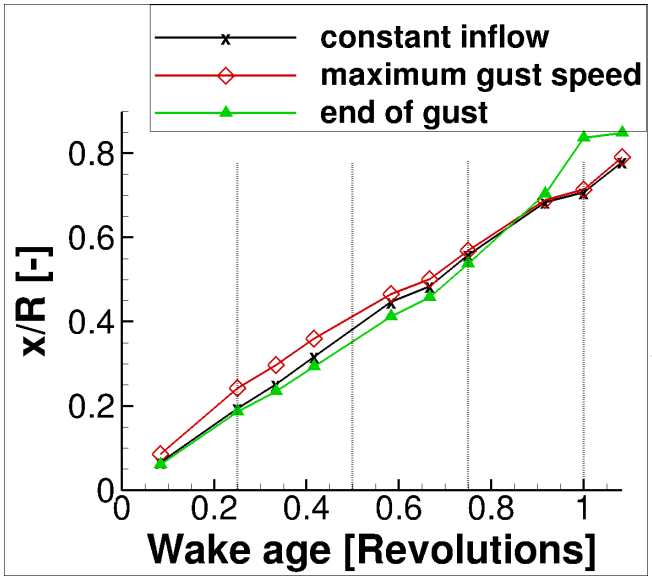

Figure 12. Tip vortex transportation in main flow direction in dependency of the wake age at three time instances during the gust

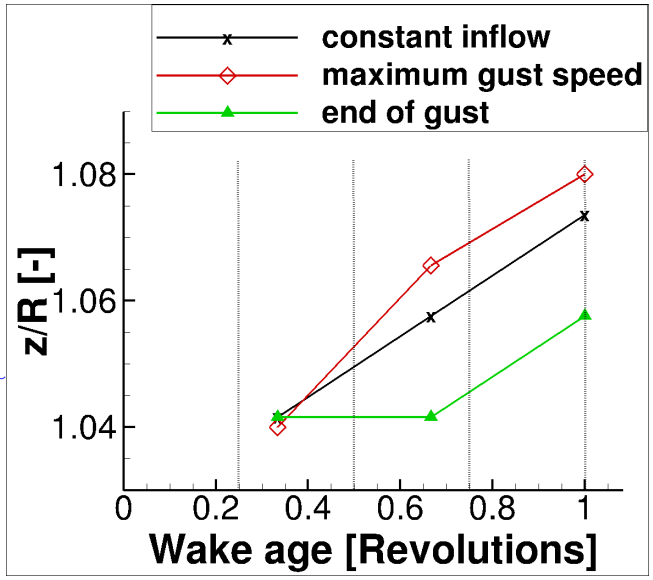

Figure 13. Tip vortex transportation vertical to main flow direction in dependency of the wake age at three time instances during the gust

Contrariwise, all existing vortices experience identical changes in the transport velocity. Thus, the geometrical distance between existing vortices remains constant.

In figure 11 three instances of the flow field are compared. In all three instances, the rotor is at $\Psi = 0°$ positions. The vortices are made visible with the λ_2 criterion (Jeong and Hussain, 1995). ~~In both figures, the black lines represent the vortex transport at~~ The black lines are extracted during constant inflow, the ~~blue~~ red lines are extracted ~~at maximum gust velocity~~ shortly before t_{max} and the green ones at the end of the gust. By comparing the vortex transport at the beginning of the gust (black curve) and at the end of the gust (green curve), a compression and stretching of the ~~vortex transport is found. This stretching relates closely to the time history of the inflow profile. The~~ distance between the vortices is found. The vortex transport in dependency of the vortex age is further discussed through figures 12 and 13. They compare the transport of the vortex in dependency of the vortex age parallel and orthogonal to the flow direction, respectively. As long as the inflow velocity is constant, the vortex transport is approximately $0.23 \cdot r/R$ parallel to the flow direction and $0.16 \cdot r/R$ orthogonal to the flow direction in a $1/3$-revolution interval. At maximum gust velocity, the constant distance between the vortices is lost. The vortices older than one revolution experienced constant inflow conditions. Thus the inter-vortex distance is constant. The vortices between 0.25 and 1 revolutions where shed during the reduced wind speed. Hence the distance parallel to the flow direction is reduced. As the downstream wake-transport decreases the orthogonal transport increases. The vortices ~~that are shed the latest are positioned at $x = -5\,\mathrm{m};\ y = -60\,\mathrm{m}$ as well as at $x = +5\,\mathrm{m};\ y = +60\,\mathrm{m}$ 14. Both vortices are transported identically at the beginning and end of the gust when the inflow velocity is identical. The two previously shed vortices around $x = 13\,\mathrm{m};\ y = -65\,\mathrm{m}$ and~~

~~$x = 27\,\mathrm{m}$; $y = -65\,\mathrm{m}$ were generated while the gust was at a lower inflow velocity (end of gust - green) or higher inflow velocity (maximum gust speed- blue). Thus, they are not transported as far (end of gust) or even further (maximum gust speed) and a slight compression and stretching towards the latest vortex is detectable~~younger than 0.25 revolutions experienced the high wind speed. Thus, the distance between the vortices parallel to the flow direction increases and the orthogonal transport decreases. At the end of the gust, reversed behaviour of the vortex transport is observed. The vortices between ~~$x = 40\,\mathrm{m}$ and $x = 55\,\mathrm{m}$ (or rather $x = 67\,\mathrm{m}$) experienced the maximum gust velocity and are stretched significantly. This behaviour has been expected if the procedure worked out fine. In figure 14 the vortices between 10 to 20 m behind the rotor have~~ 0.75 and 1 revolution were generated while the wind speed slowed down. Thus, the distance between the vortices parallel to the wind direction is increased while the orthogonal transport is decreased. Vortices up to an age of ~~a third revolution.In the time of a third revolution the blue vortex is transported about 5 m farther than the other two. This is due to the wind velocity acceleration close to the peak of the gust.~~ 0.75 revolutions have a decreased distance parallel to the wind direction while an increased distance orthogonal to the wind direction.

The aerodynamic characteristics, rotor thrust and rotor torque of course depend on the assumption of stiff rotor blades and constant rotational speed. If the rotor had finite mass and inertia or a speed control algorithm had been applied, the rotor loading during the gust would have been reduced significantly. Moreover, the symmetry of the rotor loading decreases as soon as the structure dynamics are taken into account.

6 Conclusions

The study presented the ~~simulation of the~~ validation of the resolved-gust approach that was implemented in the U-RANS-solver THETA. As test case, the generic 5MW wind turbine was computed, operating under a $1 - \cos()$-gust and an extreme operating ~~under an extreme 50 years~~ gust as defined in the ~~IEC-64100-1 standard using the U-RANS CFD solver THETA~~IEC 61400-1 (2005) standard. The gust has been introduced with the resolved-gust-approach (Kelleners and Heinrich, 2015; Reimer et al., 2015) by introducing the changing velocity at the inflow boundary ~~condition~~conditions. The gust velocity was then transported loss-free through the field with infinite speed of sound.

The results ~~obtained~~ perfectly represented the effects that are expected during the in-stationary inflow condition in combination with the given boundary conditions. Rotor thrust and rotor torque follow the gust shape ~~closely~~exactly. An analysis of the time history of rotor thrust and rotor torque during the gust show an increased rotor loading of about 100 % ~~as during~~ compared to constant inflow. Pressure distributions and friction force coefficients reveal that the flow on the rotor blades ~~during maximum gust speed~~ at maximum gust velocity is separated and thus highly in-stationary. Moreover, the effect of accelerating wind speeds was found in the rotor wake as the distance between the vortices is stretched and compressed according to the changes ~~in wind velocity~~of the wind speed.

~~As no experiment is available for validation, a final statement about the accuracy of the presented procedure has not been possible~~ The comparison of the results with the aero-elastic software FAST showed a very good agreement of rotor thrust and rotor torque during the EOG. Thus, it is a valid and accurate method to predict wind turbine loads during an EOG. Nevertheless,

a complete validation is not possible at this state as a gust experiment for a wind turbine is not available. The first mandatory step for ~~future investigations is to find means of validation. Moreover, to~~ further research on the gust simulation with U-RANS is to achieve a gust transport velocity with other than infinite speed of sound~~has to be the aim of further research~~. This may either be realized by adjustments of the ~~resolved-gust-approach presented herein or~~ resolved-gust approach, by implementing the field approach of, for example, Parameswaran and Baeder (1997), or the velocity disturbance approach of Reimer et al. (2015). A third possibility would be to introduce the fluctuating gust velocities obtained from LES ~~runs~~ computations which themselves fulfil the continuity conditions. Only then, the procedures of gust computations for wind turbines in THETA are prepared to be extended to respect atmospheric boundary layer flows or for aero-elastic analysis. The method would then enable to gain enhanced knowledge on the flow development and load distribution on rotor loads during gust excitations.

Acknowledgements. The presented work was funded by the Federal Ministry of Economic Affairs and Energy of the Federal Republic of Germany under grant number 0325719.

Data availability. Availability of NREL 5MW data from NREL reports; no other data available.

Competing interests. The author declares that she has no conflict of interest.

References

Bazilevs, Y., Hsu, M.-C., Kiendl, J., Wüchner, R., and Bletzinger, K.-U.: 3D simulation of wind turbine rotors at full scale. Part II:Fluid-structure interaction modeling with composite blades, International Journal for Numerical Methods in Fluids, 65, doi:10.1002/fld.2454, http://onlinelibrary.wiley.com/doi/10.1002/fld.2454/full, 2011.

Bierbooms, W.: Investigation of Spatial Gusts with Extreme Rise Time on the Extreme Loads of Pitch-regulated Wind Turbines, Wind Energy, 8, 17–34, doi:10.1002/we.139, 2005.

Bierbooms, W. and Drag, J.: Verification of the Mean Shape of Extreme Gusts, Wind Energy, 2, 137–150, 1999.

Castellani, F., Astolfi, D., Mana, M., Piccioni, E., Bechetti, M., and Terzi, L.: Investigation of terrain and wake effects on the performance of wind farms in complex terrain using numerical and experimental data, Wind Energy, doi:DOI: 10.1002/we.2094, http://onlinelibrary.wiley.com/doi/10.1002/we.2094/pdf, 2017.

Chow, R. and van Dam, C.: Verification of computational simulations of the NREL 5 MW rotor with focus on inboard flow separation, AIAA SciTech, 15, doi:10.1002/we.529, http://onlinelibrary.wiley.com/doi/10.1002/we.529/full, 2012.

DNVGL: Bladed, https://www.dnvgl.com/energy/generation/software/bladed/index.html, 2017.

Duque, E., Burklund, M., and Johnson, W.: Navier-Stokes and comprehensive analysis performance prediction of the NREL phase VI experiment, Journal of solar energy engineering, doi:10.1115/1.1624088, http://dx.doi.org/10.1115/1.1624088, 2003.

EASA: Certification Sepcifications for Large Aeroplanes CS 25, vol. Subpart C - Structure, European Aviation Sagety Agency, 2010.

Graf, P., Damiani, R., Dykes, K., and Jonkman, J.: Advances in the Assessment of Wind Turbine Operating Extreme Loads via More Efficient Calculation Approaches, in: 35th Wind Energy Symposium - AIAA SciTech Forum, American Institute of Aeronautics and Astronautics, doi:10.2514/6.2017-0680, http://dx.doi.org/10.2514/6.2017-0680, 2017.

Hand, L., Simms, D., Fingersh, M., Jager, D., Cotrell, J., Schreck, S., and Larwood, S.: Unsteady aerodynamics experiment phase VI: wind tunnel test configurations and available data campaign, Tech. Rep. NREL/TP-500-29955, NREL, https://www.nrel.gov/docs/fy02osti/29955.pdf, 2001.

Heinz, J., Soerensen, N., and Zahle, F.: Fluid-structure interaction computations for geomgeometric resolved rotor simulations using CFD, Wind Energy, 19, doi:10.1003/we.1976, 2016.

Hsu, M.-C. and Bazilevs, Y.: Fluid-structure interaction modeling of wind turbines: simulating the full machine, Computational Mechanics, 50, doi:10.1007/s00466-012-0772-0, https://doi.org/10.1007/s00466-012-0772-0, 2012.

IEC 61400-1: Wind turbines - Part1: Design requirements, 3rd edition, ISBN 2-8318-8161-7, 2005.

Imiela, M., Wienke, F., Rautmann, C., Willberg, C., Hilmer, P., and Krumme, A.: Towards Multidisciplinary Wind Turbine Design using High-Fidelity Methods, 33rd AIAA/ASME Wind Energy Symposium, doi:10.2514/6.2015-1462, 2015.

Jeong, J. and Hussain, F.: On the identification of a vortex, Journal of Fluid Mechanics, 285, doi:10.1017/S0022112095000462, 1995.

Johansen, J., Soerensen, N., Michelsen, J., and Schreck, S.: Detached-Eddy Simulation of flow around the NREL phase-VI blade, Wind Energy, doi:10.1002/we.63, 2002.

Jonkman, J., Butterfield, S., Musial, W., and Scott, G.: Definition of a 5-MW reference wind turbine for offshore system development, Tech. Rep. NREL/TP-500-38060, NREL, http://www.nrel.gov/docs/fy09osti/38060.pdf, 2009.

Kelleners, P. and Heinrich, R.: Simulation of Interaction of Aircraft with Gust and Resolved LES-Simulated Atmospheric Turbulence, in: Notes on Numerical Fluid Mechanics and Multidisciplinary Design, edited by Radespiel, R., Niehuis, R., Kroll, N., and Behrends, K., vol. 131 of *Advances in Simulation of Wing and Nacelle Stall*, pp. 203–222, Springer Verlag, http://elib.dlr.de/99540/, 2015.

Kessler, R. and Löwe, J.: Overlapping Grids in the DLR THETA Code, pp. 425–433, Springer International Publishing, Cham, doi:10.1007/978-3-319-03158-3_43, https://doi.org/10.1007/978-3-319-03158-3_43, 2014.

Länger-Möller, A.: Investigation of the NREL Phase VI experiment with the incompressible CFD solver THETA, Wind Energy, doi:DOI: 10.1002/we.2107, 2017.

Larsen, T. and Hansen, A.: How 2 HAWC2, the user's manual, Tech. Rep. R-1597(ver.4-6), RISO National Laboratory, Technical university of Denmark, Roskilde, Denmark, iSSN 0106-2840; ISBN 978-87-550-3583-6, 2015.

Le Pape, A. and Lecanu, J.: 3D Navier-Stokes computations of a stall-regulated wind turbine, Wind Energy, doi:10.1002/we.129, 2004.

Löwe, J., Probst, A., Knopp, T., and Kessler, R.: A Low-Dissipation Low-Dispersion Second-Order Scheme for Unstructured Finite-Volume Flow Solvers, in: Proceedings of the 53rd AIAA Aerospace Sciences Meeting, American Institute of Aeronautics and Astronautics, doi:DOI 10.2514/1.J054956, 2015.

Lynch, C. and Smith, M.: Unstructured overset incompressible computational fluid dynamics for unsteady wind turbine simulations, Wind Energy, doi:10.1002/we.1532, 2013.

Matthäus, D., Bortolotti, P., Loganathan, J., and Bottasso, C. L.: A Study on the Propagation of Aero and Wind Uncertainties and their Effect on the Dynamic Loads of a Wind Turbine, AIAA SciTech Forum, 35th Wind Energy Symposium, doi:10.2514/6.2017-1849, https://arc.aiaa.org/doi/abs/10.2514/6.2017-1849, 2017.

Mücke, T., Kleinhans, D., and Peinke, J.: Atmospheric turbulence and its influence on the alternating loads on wind turbines, Wind Energy, 14, doi:10.1002/we.422, 2011.

Murali, A. and Rajagopalan, R.: Numerical simulation of multiple interacting wind turbines on a complex terrain, Journal of Wind Engineering and Industrial Aerodynamics, 162, 57–72, doi:10.1016/j.jweia.2017.01.005, https://www.sciencedirect.com/science/article/pii/S0167610516304196, 2017.

Oe, H., Tanabe, Y., Sugiura, M., Aoyama, T., Matsuo, Y., Sugawara, H., and Yamamoto, M.: Application of rFlow3D code to performance prediction and the wake structure investigation of wind turbines, AHS 70th Annual Forum, 2014.

Pan, H. and Damodaran, M.: Parallel computation of viscous incompressible flows using Godunov-projection method on overlapping grids, International Journal for Numerical Methods in Fluids, 39, 441–463, doi:10.1002/fld.339, http://dx.doi.org/10.1002/fld.339, 2002.

Parameswaran, V. and Baeder, J.: Indical Aerodynamics in Compressible Flow Direct Computational Fluid Dynamic Calculation, Journal of Aircraft, 34, doi:10.2514/2.2146, https://doi.org/10.2514/2.2146, 1997.

Reimer, L., Ritter, M., Heinrich, R., and Krüger, W.: CFD-based Gust Load Analysis for a Free-flying Flexible Passenger Aircraft in Comparison to a DLM-based Approach, in: AIAA AVIATION 2015, http://elib.dlr.de/100537/, 2015.

Schaffarczyk, P., Schwab, D., and Breuer, M.: Experimental detection of laminar-turbulent transition on a rotating wind turbine blade in the free atmosphere, Wind Energy, 20, 211–220, doi:http://doi.org/10.1002/we.2001, 2017.

Scheurich, F. and Brown, R.: Modelling the aerodynamics of vertical-axis wind turbines in unsteady wind conditions, Wind Energy, 16, doi:10.1002/we.532, 2013.

Schulz, C., Klein, L., Weihing, P., and Lutz, T.: Investigations into the interaction of a wind turbine with atmospheric turbulence in complex terrain, Journal of physics, The science of making torque from wind (TORQUE 2016), doi:10.1088/1742-6596/753/3/032016, 2016.

Schwamborn, D., Gerhold, T., and R, H.: THE DLR TAU-CODE: RECENT APPLICATIONS IN RESEARCH AND INDUSTRY, in: ECCOMAS CFD 2006 CONFERENCE, 2006.

Sezer-Uzol, N. and Uzol, O.: Effect of steady and transient wind shear on the wake structure and performance of a horizontal axis wind turbine rotor, Wind Energy, 16, doi:10.1002/we.514, http://dx.doi.org/10.1002/we.514, 2013.

Sobotta, D.: The Aerodynamics and Performance of Small Scale Wind Turbine Starting, Ph.D. thesis, University of Sheffield, http://etheses.whiterose.ac.uk/11789/, 2015.

Soerensen, N. and Hansen, M.: Rotor performance predictions using a Navier-Stokes method, in: 1998 ASME Wind Energy Symposium Aerospace Sciences Meetings, American Institute of Aeronautics and Astronautics, doi:doi:10.2514/6.1998-25, https://doi.org/10.2514/6.1998-25, 1998.

Soerensen, N. and Schreck, S.: Transitional DDES computations of the NREL Phase-VI rotor in axial flow conditions, Journal of Physics, The science of making torque from wind, doi:http://doi.org/10.1088/1742-6596/555/1/012096, 2012.

Sprague, M., Jonkman, J., and Jonkman, B.: FAST Modular Framework for Wind Turbine Simulation: New Algorithms and Numerical Examples, AIAA SciTech, 33rd Wind Energy Symposium, doi:10.2514/6.2015-1461, https://doi.org/10.2514/6.2015-1461, 2015.

Suomi, I., Vihma, T., Gryning, S. E., and Fortelius, C.: Wind-gust parametrizations at heights relevant for wind energy: a study based on mast observations, Quarterly Journal of the Royal Meteorological Society, 139, 1298–1310, doi:10.1002/qj.2039, 2013.

Yelmule, M. and Anjuri, E.: CFD predictions of NREL phase VI rotor experiments in NASA/AMES wind tunnel, International journal of renewable energy research, doi:10.1.1.462.5540, 2013.

Zhang, X., Ni, S., and He, G.: A pressure-correction method and its applications on an unstructured Chimera grid, Computers & Fluids, 37, doi:https://doi.org/10.1016/j.compfluid.2007.07.019, http://www.sciencedirect.com/science/article/pii/S0045793007001776, 2008.